Rusinowo. The Symbolic Culture of Foragers in the Late Palaeolithic
and the Early Mesolithic. T. Płonka, K. Kowalski (eds.) Wrocław 2017, p. 119–146
DOI: 10.23734/22.18.106

Joanna Trąbska, Aleksandra Wesełucha-Birczyńska, Barbara Trybalska, Adam Gaweł

# 3.3.1. The surface of the artefact

**Abstract:** Samples extracted from the surface of the Late Palaeolithic object made of elk antler with a surface featuring dark grey and black streaks and stains were submitted for SEM/EDS analysis. The non-invasive method of Raman spectroscopy was used to preserve the integrity of the artefact. The aim of the studies was identifying the substance responsible for the stains and elucidating their origin. Substances and processes taken into account included surface treatment of the object's surface with organic acids and tannins, staining by organic pigments, an organic material holder (sheath), decomposing organic remains, or ashes from fires. The dark grey and black stains were identified by analysis as concentrations of framboidal pyrite. No evidence was found that the origin of these concentrations is other than natural.
**Keywords:** SEM/EDS, Raman micro-spectroscopy, framboidal pyrite, Late Palaeolithic, elk antler, archaeology

## Introduction

The Late Palaeolithic object from Rusinowo decorated with zigzag designs and a schematic human figure was manufactured from the elk antler (Płonka *et al.* 2011). During our study we looked for answers to the following questions: are the modifications to the surface of the object the effect of diagenetic processes? Was it exposed to deliberate action other than those involved in making and ornamenting the object? What are the possible effects of either of these two factors? Of particular interest to us was the origin of the dark grey stains and their nature. Was the antler subjected to a thermal treatment, or exposed to higher temperatures for other reasons? Was it worked in some other way, eg, by being immersed in organic substances? Was its surface coated with some substance for protective and/or aesthetic reasons? Had the object been kept safe in a sheath of some sort, made from a material of animal (skin) or plant origin? Do the diagenetic changes mask some significant information?

## Methods of research

In the present study we applied the following methods of research:

- Raman micro-spectroscopy. This method is virtually non-destructive: selected fragments of the object were placed under the lens of a microscope and irradiated with an argon laser beam, using a wavelength of 514.5 nm (Spectra-Physics Ar+ laser). The laser beam had a diameter of 1–2 micrometres (1 micrometre = $1{\cdot}10^{-6}$ m). The obtained results were documented in the form of spectra. The studies were made with Renishaw InVia Raman micro-spectrometer coupled with a Leica microscope. Raman spectroscopy has been used both in studies of bone and antler (to identify their mineral composition, the crystallinity of bioapatite, the presence of the carbonate component, collagen characteristics) and of archaeological objects made of various raw materials, and the products of their transformation induced by various factors;

J. Trąbska – University of Rzeszów Institute of Archaeology, ul. Moniuszki 10, 35-015 Rzeszów, joanna.trabska@archeologia.rzeszow.pl

A. Wesełucha-Birczyńska – Jagiellonian University Faculty of Chemistry, ul. Gronostajowa 2, 30-387 Kraków, birczyns@chemia.uj.edu.pl

B. Trybalska, A. Gaweł – AGH University of Science and Technology, al. Mickiewicza 30, 30-059 Kraków, barbara.trybalska@wp.pl, agawel@agh.uci.edu.pl

- scanning electron microscopy with an X-ray microanalyser (SEM/EDS), enabling chemical point analysis of relevant microstructure areas. These studies were made using a FEI Nano Nova scanning electron microscope coupled with an EDAX microanalyser. Not coated with graphite the samples were examined under low vacuum conditions. Samples were in the form of a small number of grains, extracted from the surface of the object with a needle, using binocular magnifying glasses. The sampling areas were documented (Tables 1, 2). This method enabled the assessment of the degree of diagenetic changes of antler apatite by analysing its micromorphology;
- X-ray diffraction (XRD) as a method supplementary to the Raman spectroscopy. Analyses were made with a Philips X'Pert PW 3020 diffractometer, using CuKα radiation. To eliminate interference from the apparatus on the intensity of analytical lines, prior to examining every sample we regulated the intensity using quartz standard reference material. Samples were in the form of several grains, extracted from the surface of the object with a scalpel, using binocular magnifying glasses. Sampling areas were documented (Tables 1, 2). The assessed stage of transformation of the bone apatite is expressed as the measured full width at half maximum (FWHM).

**Table 1.** Rusinowo. Samples investigated with SEM/EDS and XRD. Raman measurement codes are in bold and marked in italics. Areas from which samples were obtained are marked using the terminology given in sub-chapters 3.1. and 3.2.

| Area number | SEM/EDS | XRD | Raman spectroscopy |
|---|---|---|---|
| PP1 | PP1 | – | ***1*** – white, smooth, side A, above AII, 20× |
| PP2 | – | – | |
| PP3 | – | – | ***1a*** – q.v. 50× |
| PP4 | PP4 | – | |
| PP5 | PP5 | PP5 | ***2*** – dark, below BVIII, 50× |
| PP6 | – | PP6 | |
| PP7 | PP7 | PP7 | ***3*** – white, above BIV, 50× |
| PP8 | – | PP8 | |
| PP9 | – | – | ***4*** – black, next to the anthropomorphic image, 50× |
| PP10 | – | – | |
| PP11 | – | – | ***5*** – grey, side B, near the apex, NE of cavity, 50× |
| | – | – | |
| CZ1 | – | – | ***6*** – grey, side B, N of cavity, 50× |
| CZ2 | – | – | |
| CZ3 | – | – | ***6a*** – S of BVId4, 50× |
| CZ4 | CZ4 | – | ***6b*** – N of BVb30, 50× |
| CZ5 | CZ5 | – | ***7*** – black, between BVII and BVIII, 50× |
| CZ6 | CZ6 | – | |
| CZ7 | CZ7 | – | ***8*** – white, between BVI and BVII, near BVII, 50× |
| | – | – | ***9*** – white, between BIV and BV, 50× |
| | – | – | ***10*** – black, on side A, SE of AVII, 50× |
| | – | – | ***12*** – black, SW of AIII, on the rim, 50× |
| Antler of modern elk | (+) | (+) | Outer face, 50× |
| | | | Outer face, 20× |
| | | | Outer face, 20× |
| | | | Outer face, 50× |
| Silicone | – | – | Silicone |

**Table 2.** Rusinowo. Areas analysed with XRD and SEM/EDS. Approximate areas from which samples were obtained are marked with arrows. (Photo M. Diakowski)

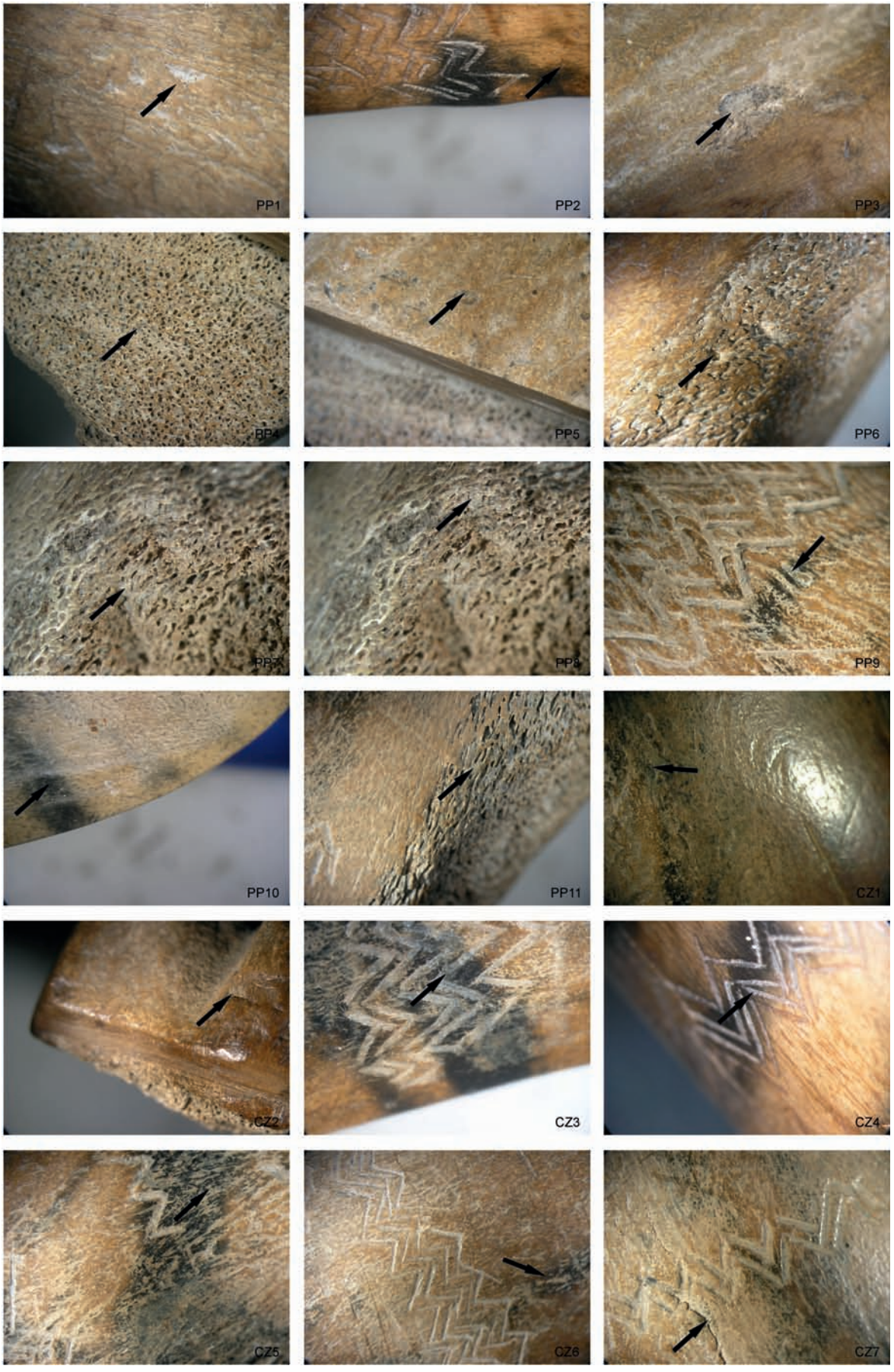

## The material

The analysed samples were extracted from the whitish-grey, dark grey and black areas on the artefact's surface. Samples for XRD and SEM/EDS analysis – a minute quantity of the material – were removed by scratching with a sterile needle. The Raman analyses were non-invasive.

A fragment of a section of a raw elk antler (sample provided by T. Płonka) was examined. The surface of the antler was analysed using the method of Raman spectroscopy. A sample of some bulk volume (thus, representing both the surface and the interior) was extracted for XRD analysis. Additionally, studies were made of silicone used previously (prior to the making of analyses made within the present study) in making a cast of the artefact, to eliminate possible signals deriving from contamination with resin.

Information about the type of the tested samples is given in Table 1. The spots studied via spectroscopy analyses and via SEM/EDS are not the same due to the restricted possibility of placing and immobilizing the object under the laser beam. Information about microscope magnifications (× 20 and × 50) used when scanning with the laser beam is included in the table.

### XRD study results

The results of the study of the phase composition and crystallite size of apatite in the modern antler and in the artefact are given in Table 3. The FWHM measurement of the reflex of 2.8 Å of apatite for samples PP4-PP8 extracted from the ancient object may be weighed with error due to the extremely small sample size.

The sample analysed via XRD was very small, making interpretation difficult. Nevertheless, the results obtained were satisfactory. The samples are composed chiefly of apatite (hydroxyapatite and fluoroapatite), except for the modern antler which contained a small amount of quartz, and sample PP4, which contained calcite. The FWHM measurement of the reflex of apatite suggests a very low crystallinity, but still a little higher than the crystallinity in the modern antler.

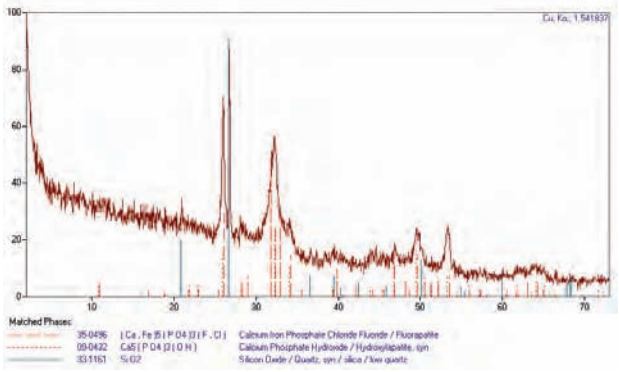

**Fig. 1.** Rusinowo. Diffractogram obtained for modern elk antler sample

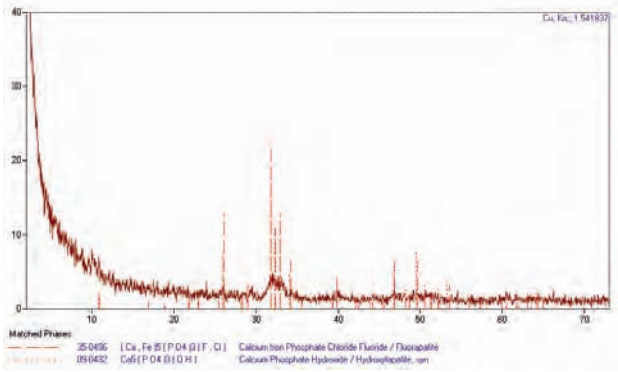

**Fig. 3.** Rusinowo. Diffractogram obtained for sample PP8 from area BIV of the object, white fragment

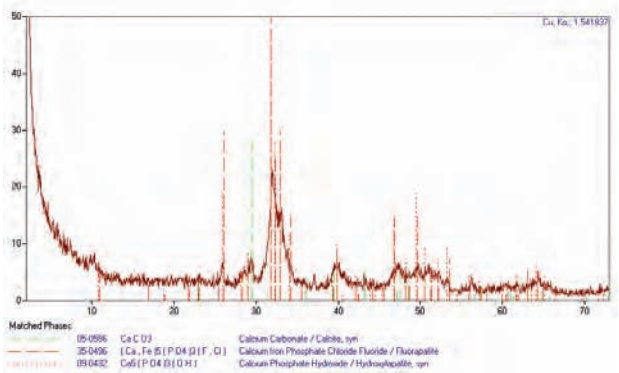

**Fig. 2.** Rusinowo. Diffractogram obtained for sample PP4 from side A of the artefact, white fragment

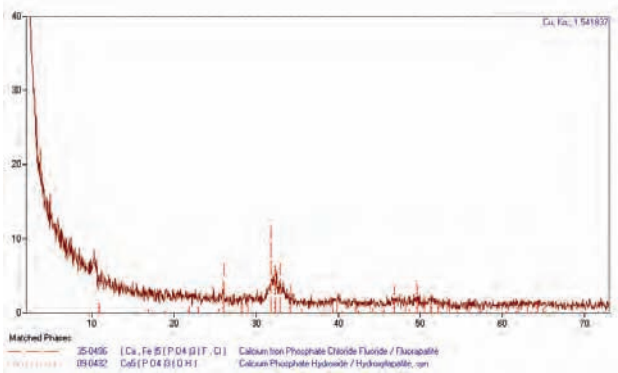

**Fig. 4.** Rusinowo. Diffractogram obtained for sample PP5 from area BVIII of the object, dark fragment

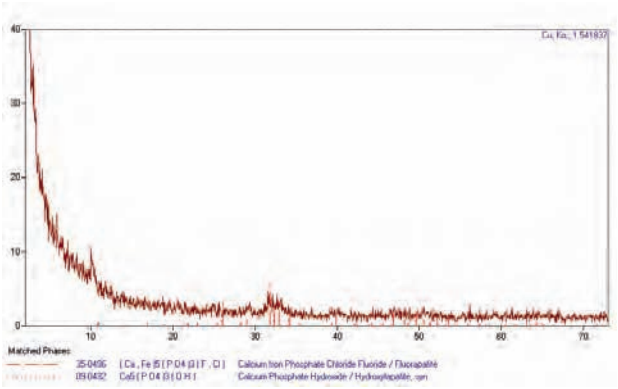

**Fig. 5.** Rusinowo. Diffractogram obtained for sample PP6 from area BVIII of the object, dark fragment

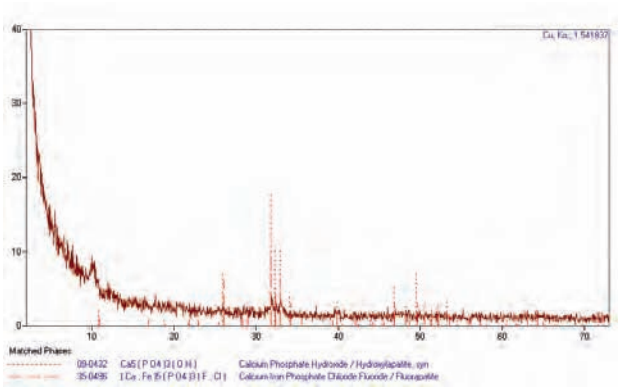

**Fig. 6.** Rusinowo. Diffractogram obtained for sample PP8 from area BIV of the object, dark fragment

**Table 3.** Rusinowo. Results of phase studies and apatite crystallite size measurement. Numbers in brackets correspond to data from ICDD database (International Centre for Diffraction Data, 2005)

| Sample | Phase composition | Full width at half maximum (FWHM) of reflex 2.8Å [2θ] |
|---|---|---|
| Elk antler | Apatite (35-496), (9-432) – weakly crystalline, quartz (33-1161) – a trace. | ca. 1.1o |
| White and light grey area | | |
| PP4 | Apatite (35-496), (9-432) – weakly crystalline, calcite (5-586). | ca. 1.7o |
| PP7 | Apatite (35-496), (9-432) – weakly crystalline. | ca. 2.12o |
| Black and dark grey area | | |
| PP5 | Apatite (35-496), (9-432) – weakly crystalline. | ca. 1.9o |
| PP6 | Apatite (35-496), (9-432) – weakly crystalline. | ca. 1.9o |
| PP8 | Apatite (35-496), (9-432) – weakly crystalline. | ca. 1.8o |

## Spectroscopy study results

The spectra collected from the surface of the object are presented in Figs. 7–18, for modern elk antler in Figs. 19–21, for silicone in Fig. 22. The list of the recorded bands is given in Table 4.

The two main components of the antler and of the archaeological object are bioapatite (biogenic apatite with carbonate group substitutions) and collagen. The bands from apatite of the phosphate group were identified at 432, 449 (vibrations ν2), 581, 592, 608 and 617 (vibrations ν4), 965 (vibration ν1), 1034, 1042, 1053, 1061 and 1081 $cm^{-1}$ (vibrations ν3) (Penel *et al.* 1997). The shape of the spectra can be viewed in the cited study and eg, in the database of the RRUFF Project (http://rruff.info). The range of vibrational variation is shown in Table 6. Sharp bands

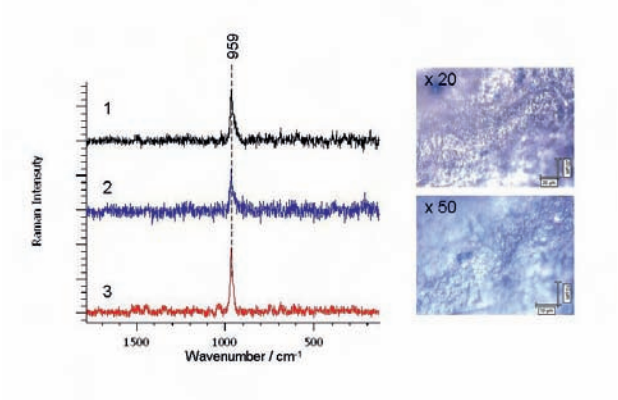


**Fig. 7.** Rusinowo. Spectrum for point 1 (dark blue and black) and 1a (red). Smooth, white area

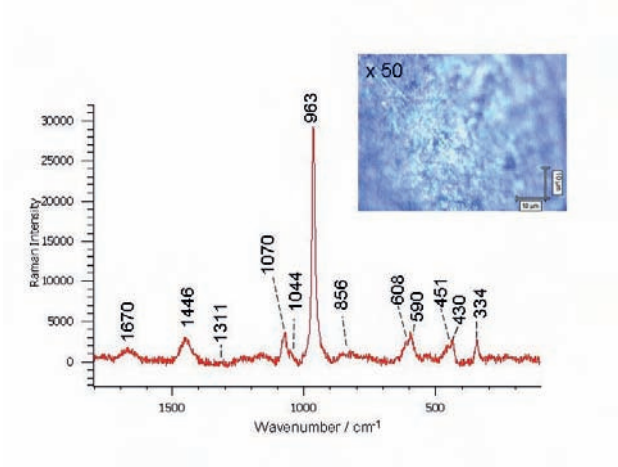


**Fig. 8.** Rusinowo. Spectrum for point 2. Dark area

characterise a mineral with an ordered crystalline structure. The bands from collagen are at 1664, 1460, 1302, 1266, 1246, 1163, 1129, 1030, 1004, 937, 918, 873, 856, 815, 667 and 646 $cm^{-1}$. The interpretation of the vibrations and their variation range dependent on the origin of the collagen were collected in Table 7. The shape of the spectra is in agreement with the literature cited in Table 7. Bands from other identified phases were collected in tables given in the "Discussion" section.

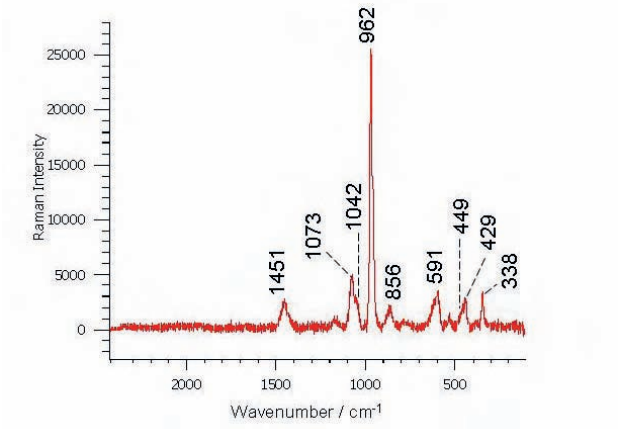


**Fig. 9.** Rusinowo. Spectrum for point 2a, magnified 50×

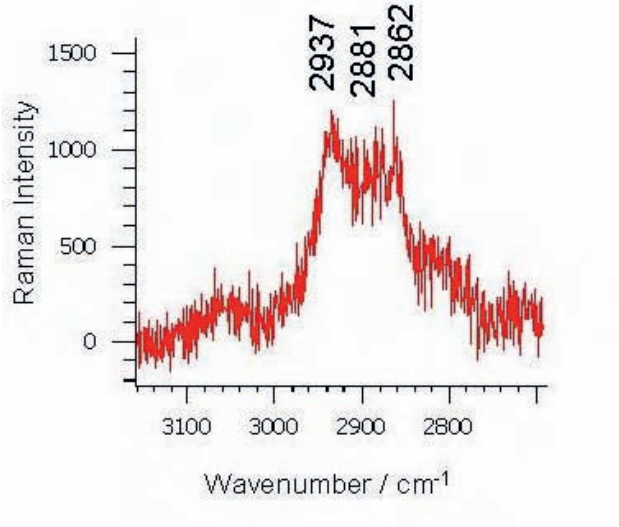


**Fig. 10.** Rusinowo. Spectrum for point 2a, magnified 50×, Raman shift range 2800–3100 $cm^{-1}$

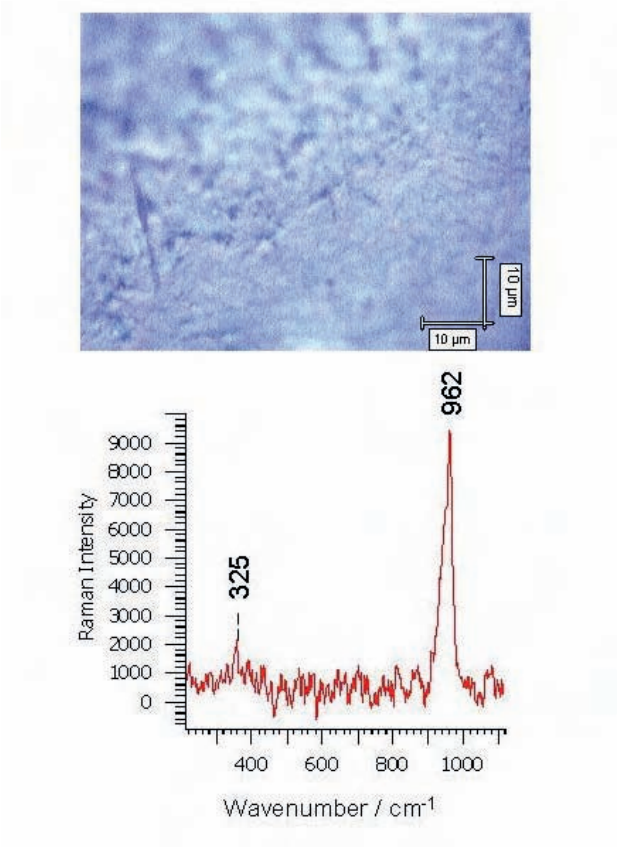


**Fig. 11.** Rusinowo. Spectrum for point 3, white area

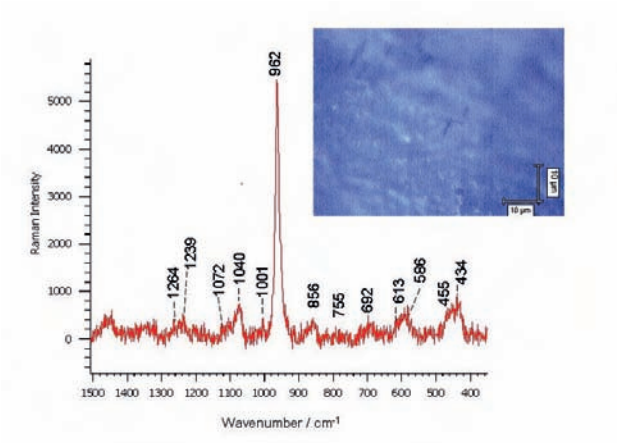


**Fig. 12.** Rusinowo. Spectrum for point 5, grey area

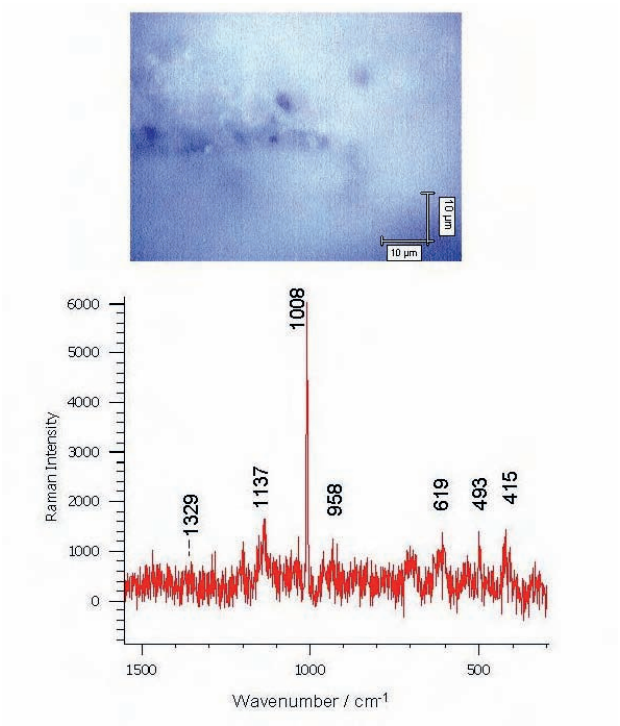


**Fig. 13.** Rusinowo. Spectrum for point 6, grey area

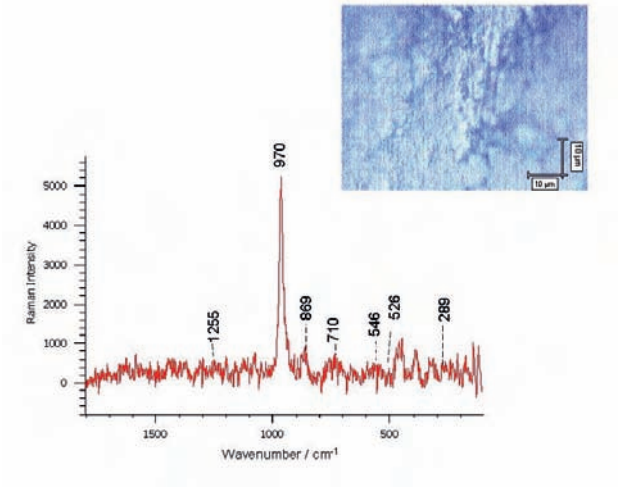


**Fig. 14.** Rusinowo. Spectrum for point 8, white area

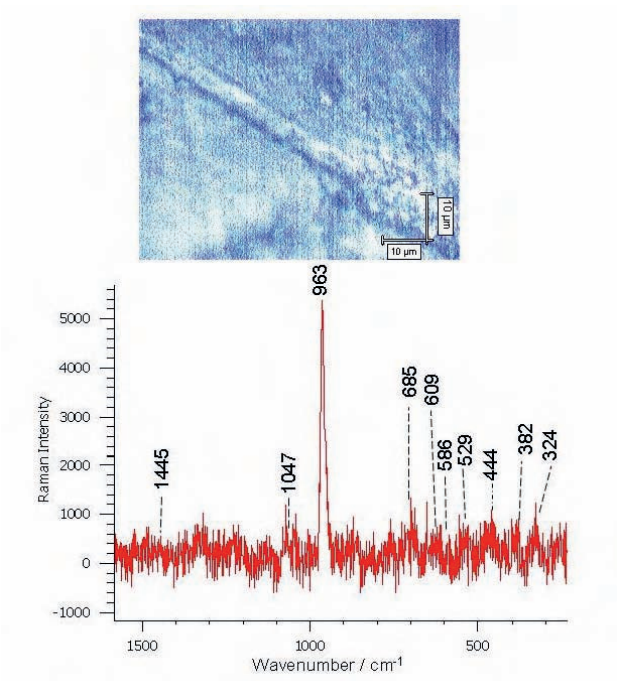


**Fig. 15.** Rusinowo. Spectrum for point 9, white area next to ornament groove

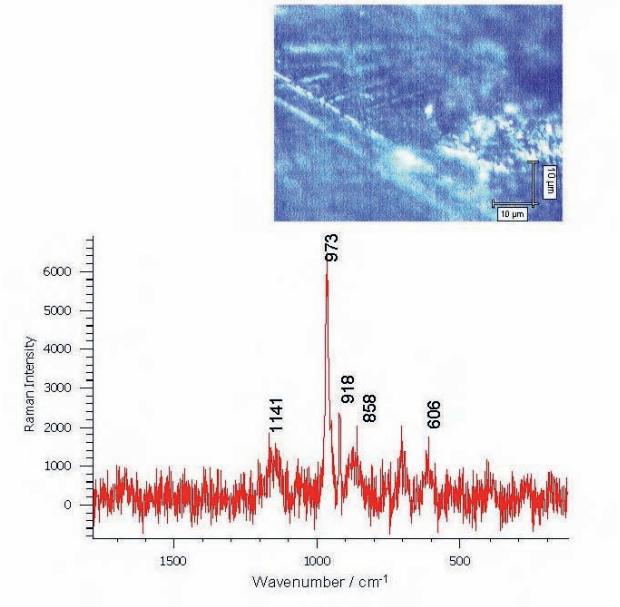


**Fig. 16.** Rusinowo. Spectrum for point 10, black area next to ornament groove

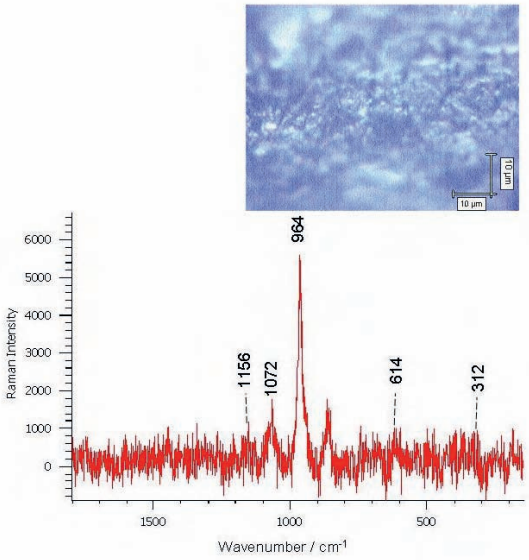


**Fig. 17.** Rusinowo. Spectrum for point 12, black area

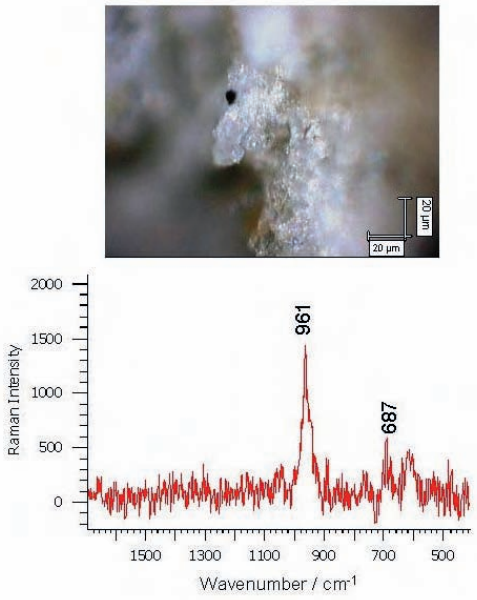


**Fig. 18.** Spectrum for modern elk antler. Outer face

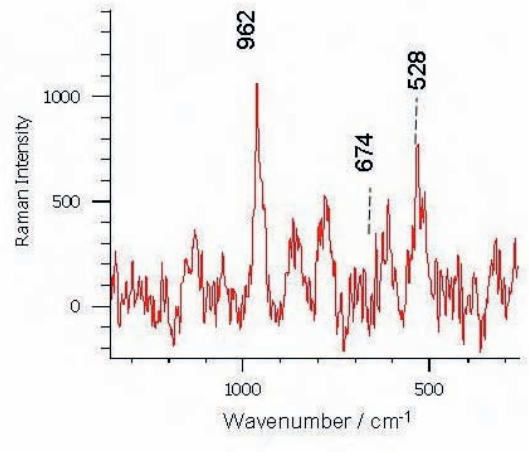


**Fig. 19.** Spectrum for modern elk antler. Outer face. Magnified 20×

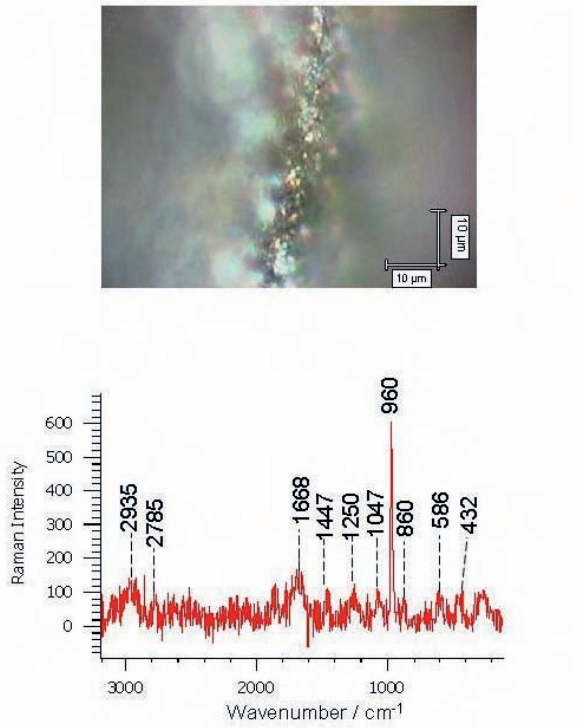


**Fig. 20.** Spectrum for modern elk antler. Outer face

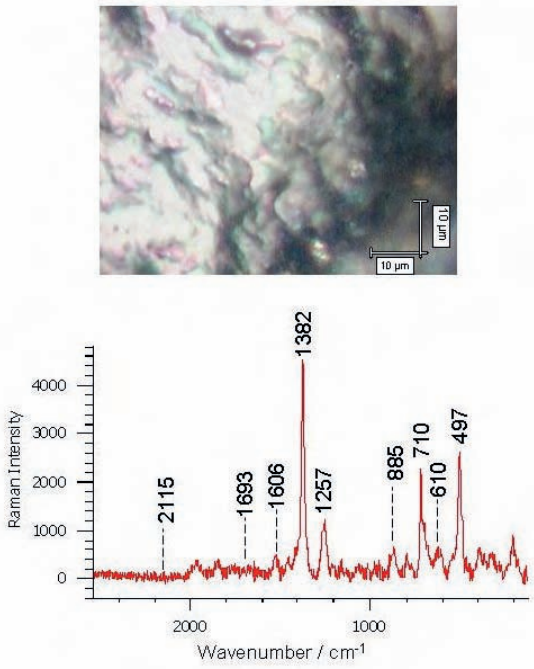


**Fig. 21.** Spectrum for silicone

**Table 4.** Rusinowo. Raman vibrations from investigated samples [$cm^{-1}$]. HA – hydroxyapatite. Most of the source literature used during interpretation is listed in tables 6–8

| Samples from the artefact | | | | | | | | | | Antler of modern elk | | | | Interpretation |
|---|---|---|---|---|---|---|---|---|---|---|---|---|---|---|
| 1 | 2 | 2a | 3 | 5 | 6 | 8 | 9 | 10 | 12 | Antler, outer face, top | Antler, outer face top | Antler outer face 1 | Silicone | |
| – | – | – | – | – | – | 289 | – | – | – | – | – | – | – | Moderately crystalline mackinawite |
| – | – | – | – | – | – | – | – | – | 312 | – | – | – | – | Fe(III) compounds containing mackinawite |
| – | – | – | 325 | – | – | – | 324 | – | – | – | – | – | – | Pyrite, Fe(III) compounds containing mackinawite |
| – | 334 | 338 | – | – | – | – | – | – | – | – | – | – | – | Pyrite, possibly greigite |
| – | – | – | – | – | – | – | 382 | – | – | – | – | – | – | Pyrite, Fe(III) compounds containing mackinawite |
| – | – | – | – | – | 415 | – | – | – | – | – | – | – | – | Gypsum |
| – | – | 421 | – | – | – | – | – | – | – | – | – | – | – | Greigite |
| – | 430 | 429 | – | 434 | – | – | – | – | – | – | – | 432 | – | Pyrite, HA |
| – | – | 449 | – | – | – | – | 444 | – | – | – | – | – | – | HA |
| – | 451 | – | – | 455 | – | – | – | – | – | – | – | – | – | HA |
| – | – | – | – | – | 493 | – | – | – | – | – | – | – | 497 | Gypsum, silicone |
| – | – | – | – | 520 | – | 526 | 529 | – | – | – | 528 | – | – | Secondary calcium phosphates |
| – | – | – | – | – | – | 546 | – | – | – | – | – | – | – | Secondary calcium phosphates? |
| – | 590 | – | – | 586 | – | – | 586 | – | – | – | – | 586 | – | HA |
| – | | 591 | – | | – | – | | – | – | – | – | – | – | HA, collagen |
| – | 608 | | – | 613 | – | – | 609 | 606 | | | | – | – | Collagen |
| – | – | – | – | – | 619 | – | – | – | 614 | – | – | – | 610 | Gypsum, silicone |
| – | – | – | – | – | – | – | – | – | – | – | 674 | – | – | Collagen |
| – | – | – | – | – | – | – | 685 | – | – | 687 | – | – | – | Secondary calcium phosphates? |
| – | – | – | – | 692 | – | – | – | – | – | – | – | – | – | Secondary calcium phosphates? |
| – | – | – | – | – | – | 710 | – | – | – | – | – | – | 710 | Secondary calcium phosphates? Silicone |
| – | – | – | – | 755 | – | – | – | – | – | – | – | – | – | Collagen |
| – | 856 | 856 | – | 856 | – | 869 | – | 858 | – | – | – | 860 | – | HA, collagen |

| Samples from the artefact | | | | | | | | | | Antler of modern elk | | | | Interpretation |
|---|---|---|---|---|---|---|---|---|---|---|---|---|---|---|
| 1 | 2 | 2a | 3 | 5 | 6 | 8 | 9 | 10 | 12 | Antler, outer face, top | Antler, outer face top | Antler outer face 1 | Silicone | |
| – | – | – | – | – | – | – | – | | – | – | – | – | 885 | Silicone |
| – | – | – | – | – | – | – | – | 918 | – | – | – | – | – | Organic substance (acetates?) (Ito, Bernstein 1956) |
| 959 | 963 | 962 | 962 | 962 | 958 | 970 | 963 | 973 | 964 | 961 | 962 | 960 | – | HA |
| – | – | – | – | 1001 | – | – | – | – | – | – | – | – | – | Gypsum? |
| – | – | – | – | – | 1008 | – | – | – | – | – | – | – | – | Gypsum |
| – | 1044 | 1042 | – | 1040 | – | – | 1047 | – | – | – | – | 1047 | – | HA |
| – | 1070 | 1073 | – | 1072 | – | – | – | – | 1072 | – | – | – | – | HA, ν3CO3 2– (type B) vibration |
| – | – | – | – | – | 1137 | – | – | 1141 | 1156 | – | – | 1156 | – | HA, gypsum |
| – | – | – | – | 1239 | – | – | – | | | – | – | | – | Collagen |
| – | – | – | – | | – | 1255 | – | – | – | – | – | 1250 | 1257 | Collagen, silicone |
| – | – | – | – | 1264 | – | – | – | – | – | – | – | – | – | Collagen |
| – | 1311 | – | – | | – | – | – | – | – | – | – | – | – | Collagen |
| – | – | – | – | – | 1329 | – | – | – | – | – | – | – | – | Organic substance (acetates?) (Ito, Bernstein 1956) |
| – | – | – | – | – | – | – | – | – | – | – | – | – | 1387 | Silicone |
| – | 1446 | – | – | 1449 | – | – | 1445 | – | – | – | – | 1447 | – | Collagen |
| – | – | 1451 | – | – | – | – | – | – | – | – | – | – | – | Collagen? |
| – | – | – | – | – | – | – | – | – | – | – | – | – | 1606 | Silicone |
| – | 1670 | – | – | 1671 | – | – | – | – | – | – | – | 1668 | – | Collagen |
| – | – | – | – | | – | – | – | – | – | – | – | – | 1693 | Silicone |
| – | – | – | – | | – | – | – | – | – | – | – | – | 2115 | Silicone |
| – | – | – | – | | – | – | – | – | – | – | – | 2785 | – | Collagen |
| – | – | 2862 | – | – | – | – | – | – | – | – | – | – | – | Organic substance, C–H vibrations |
| – | – | 2881 | – | – | – | – | – | – | – | – | – | – | – | Organic substance, C–H vibrations |
| – | – | 2937 | – | – | – | – | – | – | – | – | – | 2935 | – | Organic substance, C–H vibrations |

**SEM/EDS study results**

Samples subjected to the study were extracted from the pale, whitish-grey and black areas on the surface of the antler find. Raw antler samples were also tested. The observed results were collected in table form (Table 5) and recorded in micrographs (Figs. 22–38). The apatite in modern antler is characterized by cryptocrystalline and having a large specific surface area (Figs. 22, 23, 32). Figure 23 shows fibrillous clusters of collagen. A section through the antler reveals differences in morphology and chemical composition (Figs. 26–28). Heterogeneous clusters (points 1 and 3 in Fig. 26) are concentrations of tricalcium phosphate with subsidiary silicon, aluminium, sodium, magnesium, sulphur and iron. In the heterogeneous part (point 2 in Fig. 26) the concentration of silicon, aluminium and iron is decidedly greater.

*Modern elk antler*

As may be seen in the SEM image, the structure of the raw antler surface is needle-like and chaotic (Figs. 22, 23). The bioapatite and collagen form fine fibrils (Fig. 23). Visible in the section are homogenous zones almost purely made up of apatite (Figs. 24, 25, 27), and others additionally containing silica, visible as a more grainy aggregate (Figs. 24, 25). The Ca/P ratio is approximately 1. Carbon is present everywhere, which is the result of the presence of collagen.

*The antler object; white and light grey areas*

The examination was made of the white and whitish-grey areas on the artefact. As shown in the SEM image, the white areas are built of fibrillous bioapatite and collagen fibrils (Figs. 31, 32). The presence of apatite is manifested in EDS spectra as signals from calcium and phosphorus, the presence of collagen is revealed by the characteristic morphology of the compliant fibrils and an EDS signal from carbon. Pyrite is present here, in the form of individual fine framboidal clusters (Figs. 28, 29, 33–35) filling the cavities in the antler object, and of octahedral crystals of pyrite which fill micrometre-sized fissures in the bioapatite. Several micrometres in diameter, the framboids are built of octa- and tetrahedral crystals of pyrite with a size of about 2 micrometres. The Ca/P ratio is variable: it ranges between 1.4 and 7. In sample PP1 its value is 1.4, in sample PP4 – 1.4, 2.3 and 7. Carbon is present everywhere, in a quantity larger than could be the result of coating the samples with graphite.

*The antler object, black and dark grey areas*

In the black and dark grey areas, macroscopically having the form of maculae and smudges, we observed a large number of occurrences of framboidal pyrite (Figs. 36–45) and isolated euhedral crystals of

**Table 5.** Rusinowo. Results of SEM/EDS observation of samples obtained from different parts of the antler

| Sample | Observations |
|---|---|
| Raw antler – surface | On surface of modern antler, needle-like crystals consisting of calcium phosphate, under greater magnification found to contain very fine, individual crystals of apatite and collagen fibrils. |
| Raw antler – interior | Here only the chemical composition was recovered – typical for an osseous substance. |
| Raw antler – section | Seen in a section, dark clusters (visible at to of the photograph): they consist of a mixture of apatite and silica, and iron compounds. |
| PP1 | The apatite is very finely-crystalline, in this image nearly amorphous, with flaky crystals measuring a few micrometres. |
| PP4 | The white sample contained individual clustery, framboidal concentrations of pyrite ($FeS_2$) crystals. |
| PP5 | As above, the white powder was found to contain concentrations of framboidal pyrite. Apatite crystals were very small, in the order of 10 micrometres. The fibrous structures are identified as collagen. |
| PP7 | The sample contains very small, fibrous structures: of collagen or other organic component of the antler (cf. esp. p.1 on photographic image 12 000×). |
| CZ4 | Here we identified (lumpy) concentrations of silica and iron compounds and calcium carbonate. Also present were amorphous (globular) concentrations of organic compounds and concentrations of pyrite. |
| CZ5 | The main substance observed here was pyrite. |
| CZ6 | Here we identified the presence of an amorphous organic substance and amorphous silica. |
| CZ7 | The sample contains fibrous crystals of calcium carbonate, several hundred micrometres in size, concentrations of silica, cubic pyrite crystals scattered within the apatite and very finely crystalline apatite. Also present is an encrustation of manganese compounds. |

the mineral (Fig. 44). The pyrite is found in cavities, crevasses and on the surface of the artefact. In size the framboids reach several micrometres, the size of individual crystals ranges from 1 to 3 micrometres. Also present are some individual octahedral euhedral crystals of pyrite between 1 and 3 micrometres in size. Concentrations of framboids may be accompanied by cryptocrystalline calcium carbonate, manganese compounds and an organic substance (Fig. 46). The Ca/P ratio for all the samples ranges between 0.5 and 6. In sample PP5 it is 1.2, in PP6 – 1, 1.2; and1,4, in PP7 – 1.2, 1.4, 2, 2.1, in CZ4 – 2, in CZ5 – 1.1, in CZ7 – 0.5, 1.4, 1.5, 3, 6.

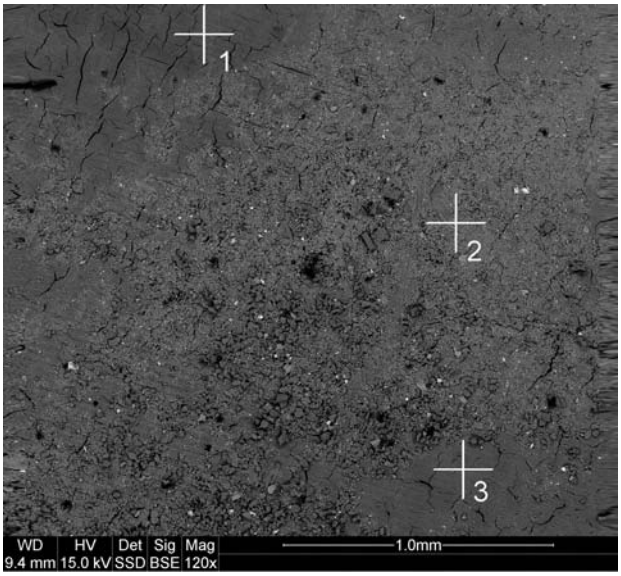


**Fig. 24.** Raw antler, cross-section. Differences in chemical composition observed at individual points (EDS spectra in Figs 25–27)

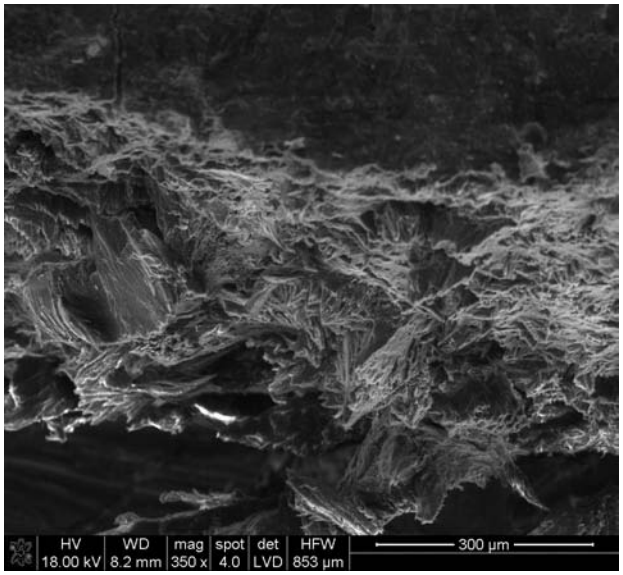


**Fig. 22.** Raw antler – surface. The needle-like and chaotic structure of bioapatite is visible

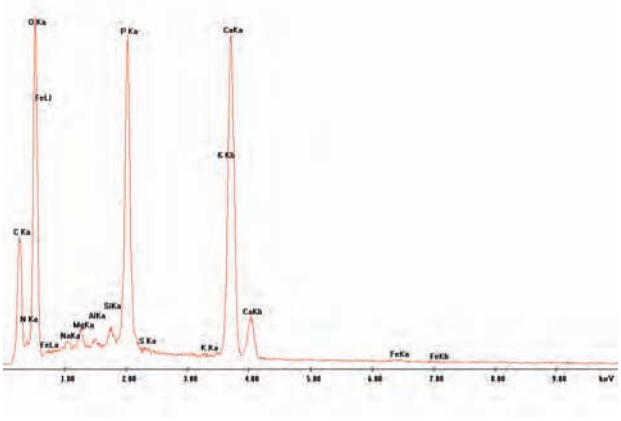

**Fig. 25.** EDS spectrum for point 1. Area of main concentrations of bioapatite

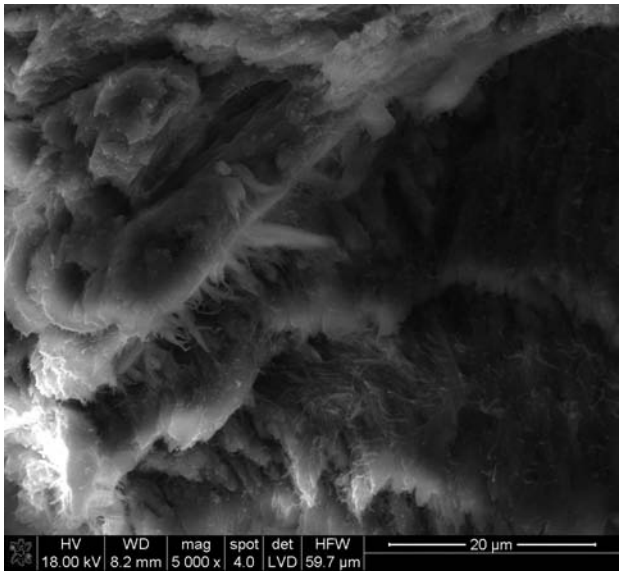


**Fig. 23.** Raw antler – fragment of surface. Fine fibrils of collagen are visible

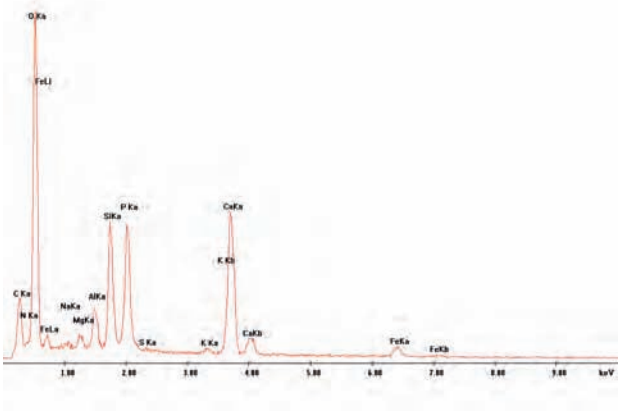

**Fig. 26.** EDS spectrum for point 2. Area of main concentration of bioapatite and $SiO_2$

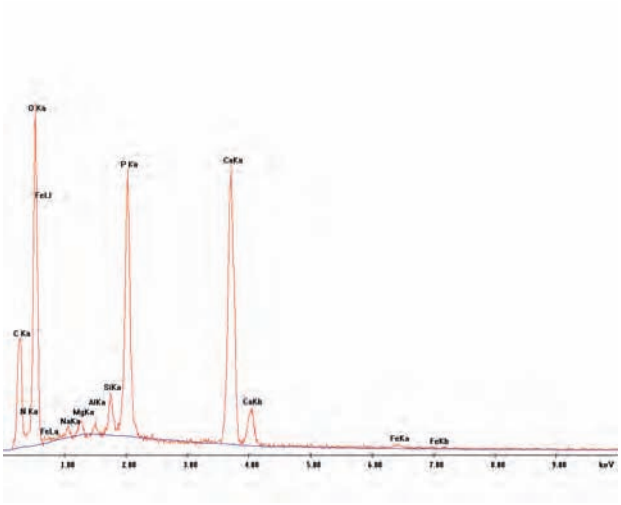


**Fig. 27.** EDS spectrum for point 3. Area of main concentration of bioapatite

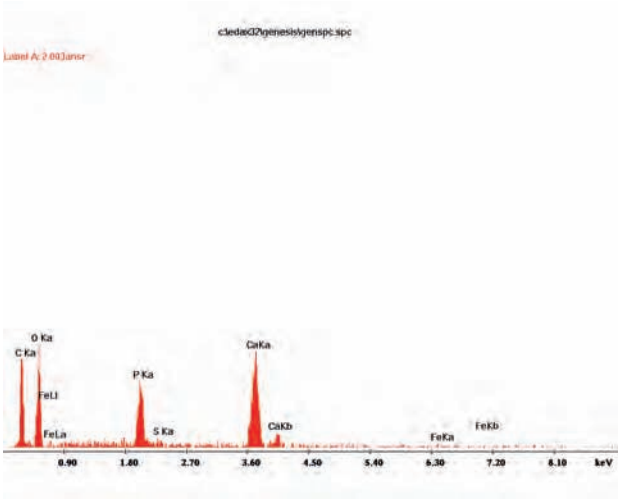


**Fig. 30.** Rusinowo. EDS spectrum obtained for areas around pyrite

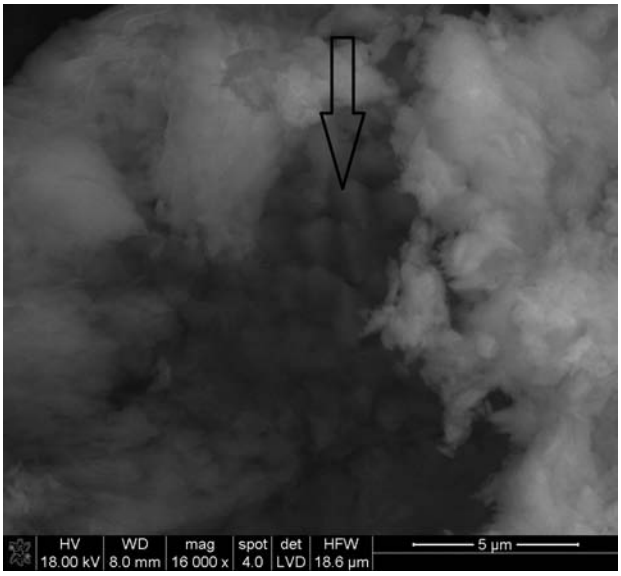


**Fig. 28.** Rusinowo. Sample PP1. Microcrystals of pyrite filling the fissures in the bioapatite (arrow)

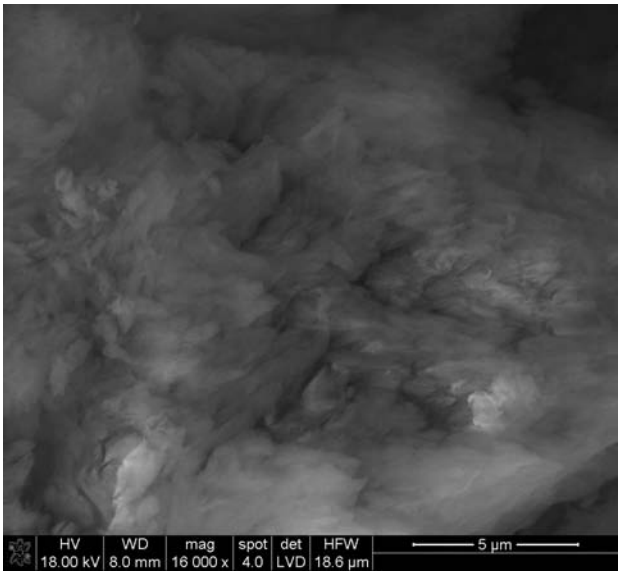


**Fig. 31.** Rusinowo. Fragment of white surface of the object with fibrillous bioapatite and collagen

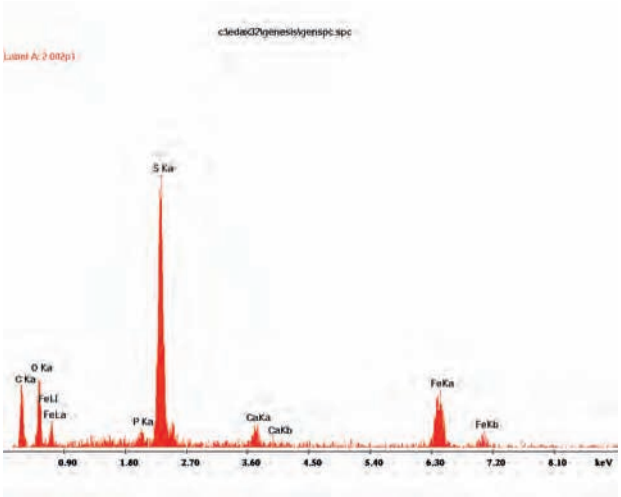


**Fig. 29.** Rusinowo. EDS spectrum obtained for area in Fig. 28 area indicated by arrow

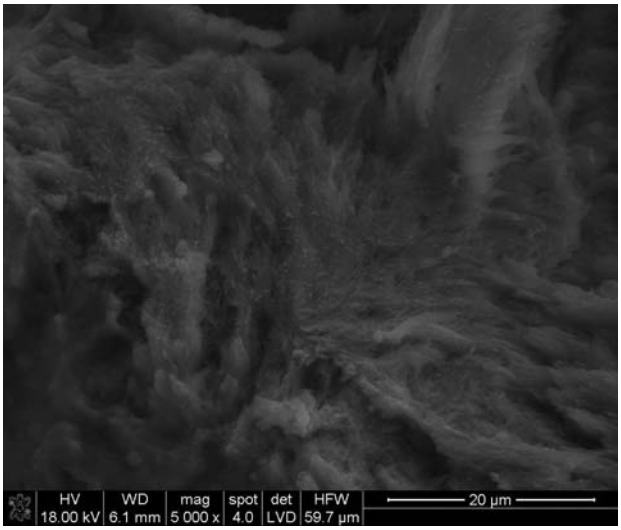


**Fig. 32.** Rusinowo. Sample PP1. Fragment of fibrillous bioapatite and collagen

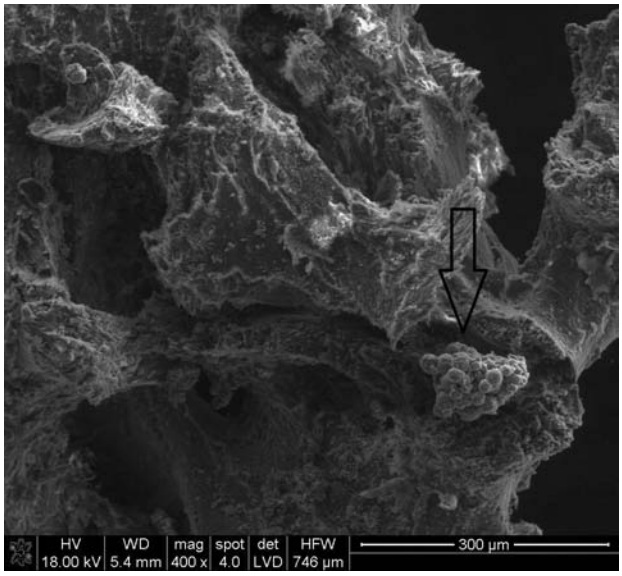


**Fig. 33.** Rusinowo. Sample PP1. Concentrations of framboidal pyrite (arrow) within the white fragment of the object

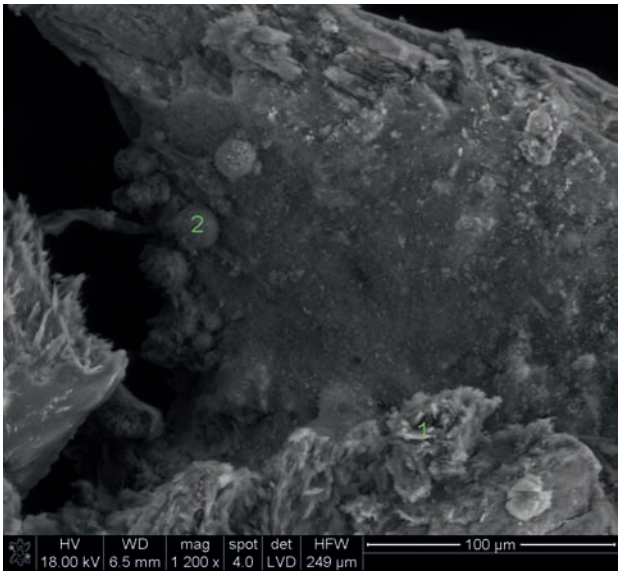


**Fig. 36.** Rusinowo. Sample PP5, for point 1: microstructure of the dark area, for point 2: concentration of framboidal pyrite

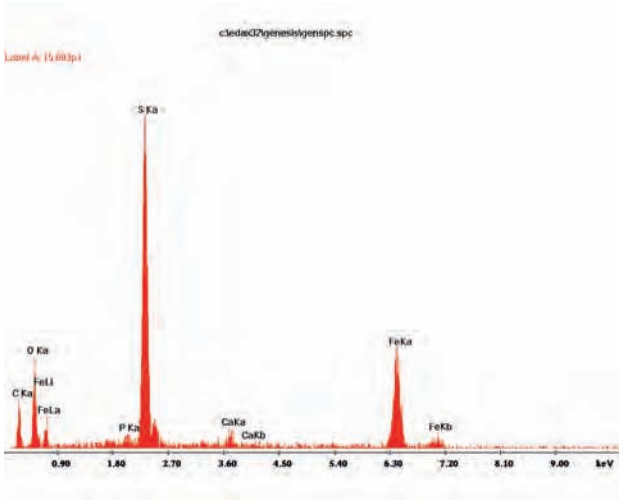


**Fig. 34.** Rusinowo. EDS spectrum obtained for pyrite framboids

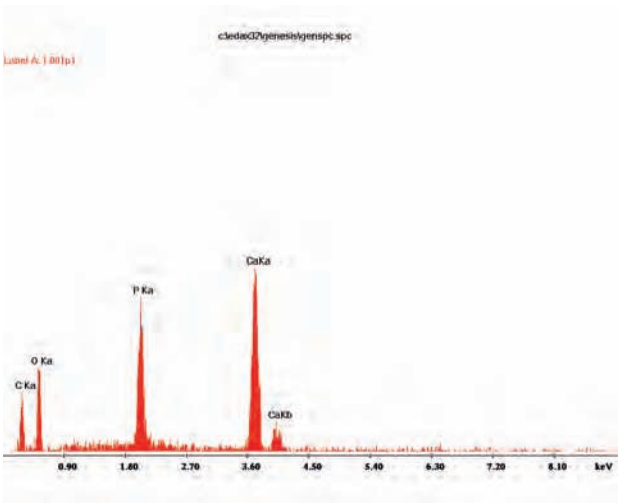


**Fig. 37.** Rusinowo. EDS spectrum obtained for point 1. Concentration of bioapatite, and possibly calcium carbonate

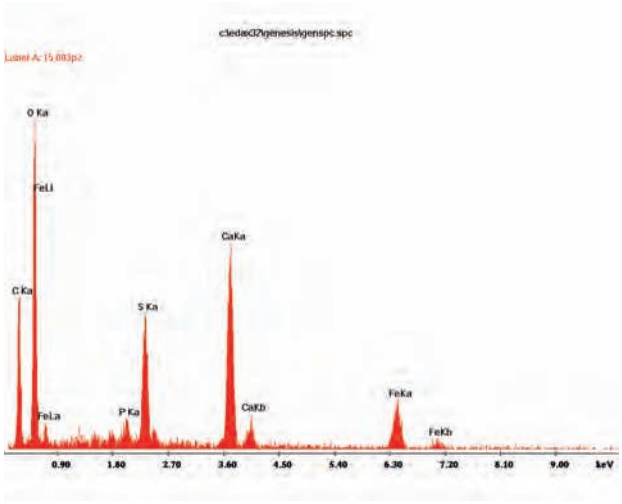


**Fig. 35.** Rusinowo. EDS spectrum obtained for fine, irregular concentrations between the framboids. There is an observable high concentration of calcium and negligible concentration of phosphorus

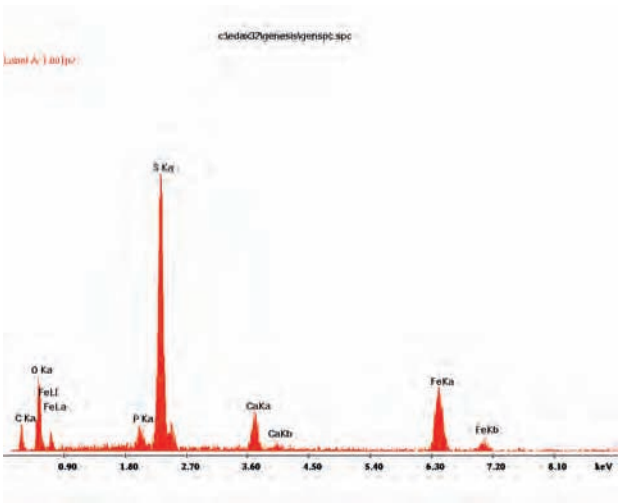


**Fig. 38.** Rusinowo. EDS spectrum obtained for point 2. Concentration of iron sulphide(s), bioapatite, and possibly calcium carbonate

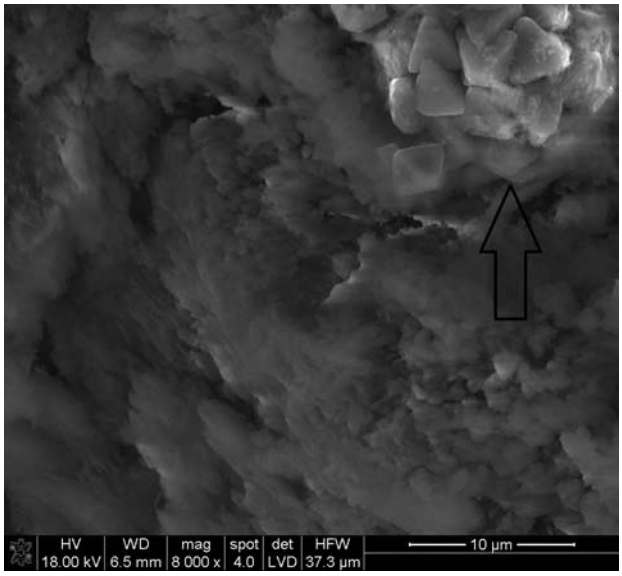


**Fig. 39.** Rusinowo. Sample PP5, close up of microstructure of dark area of the object and framboid built by tetrahedral (presumably, also octahedral) pyrite crystals (arrow)

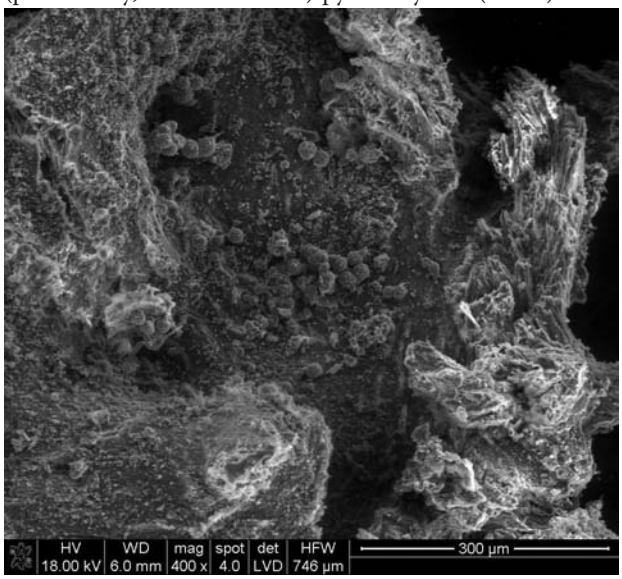


**Fig. 40.** Rusinowo. Sample CZ7. Framboidal pyrite scattered inside caverns of the object

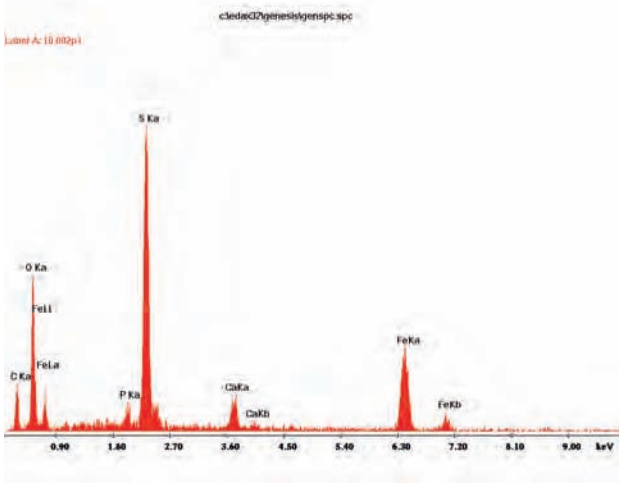


**Fig. 41.** Rusinowo. EDS spectrum obtained for point 1. Concentration of iron sulphide(s), bioapatite, and possibly calcium carbonate

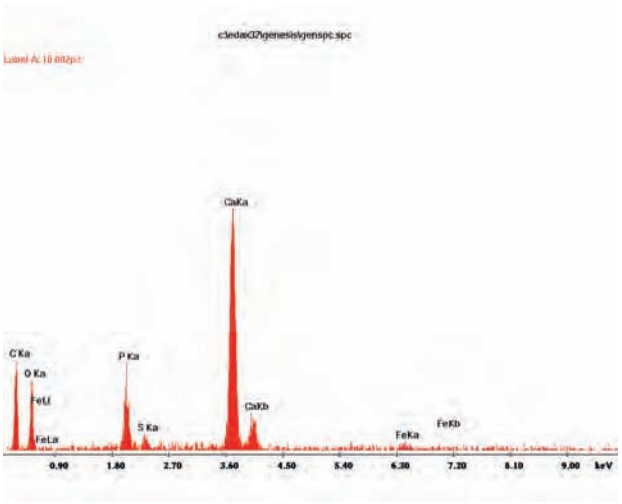


**Fig. 42.** Rusinowo. EDS spectrum obtained for point 2. Concentration of bioapatite and calcium carbonate

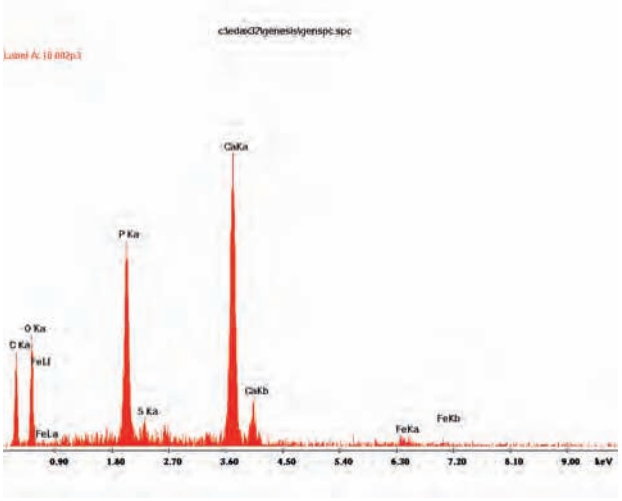


**Fig. 43.** Rusinowo. EDS spectrum obtained for point 3. Concentration of bioapatite and calcium carbonate

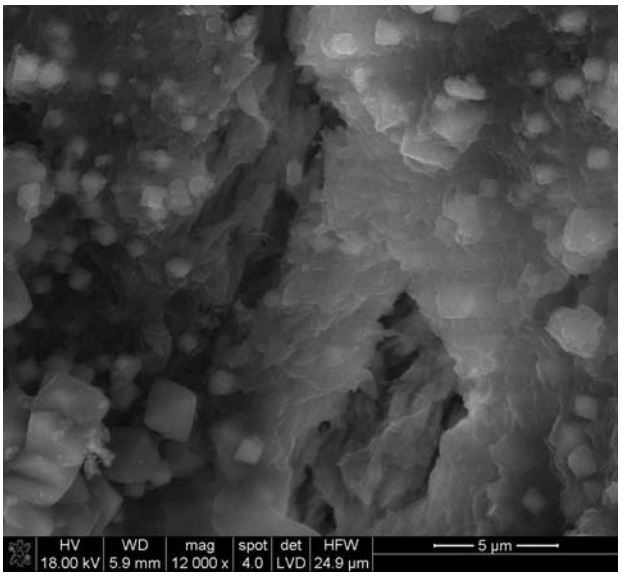


**Fig. 44.** Rusinowo. Sample CZ7. Crystalline pyrite scattered in the form of individual octahedral crystals. The same sample contained also framboidal pyrite

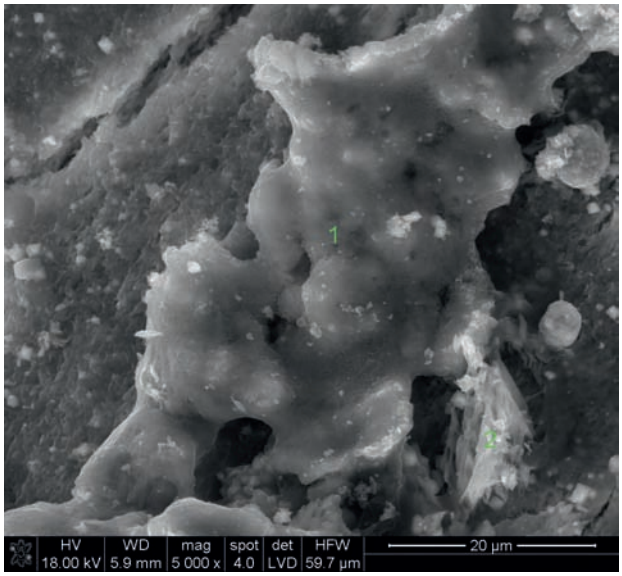


**Fig. 45.** Rusinowo. Sample CZ7. Encrustation of manganese compounds (marked as point 1). At point 2 next to calcium carbonate, a minor concentration of pyrite and bioapatite

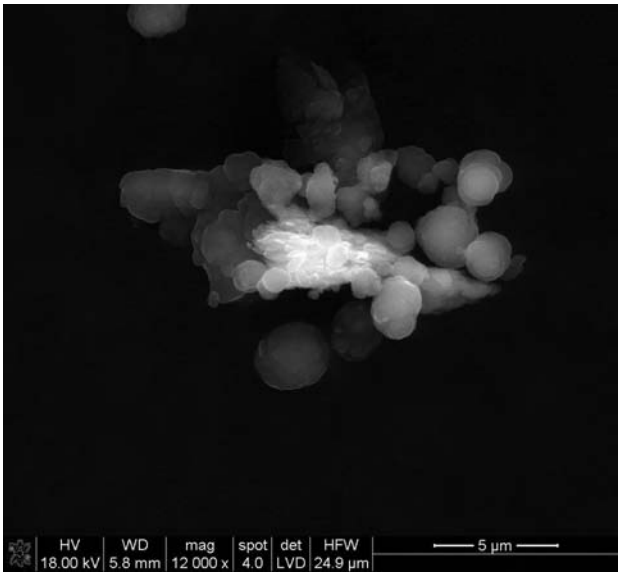


**Fig. 46.** Rusinowo. Sample CZ4. A concentration of organic compounds

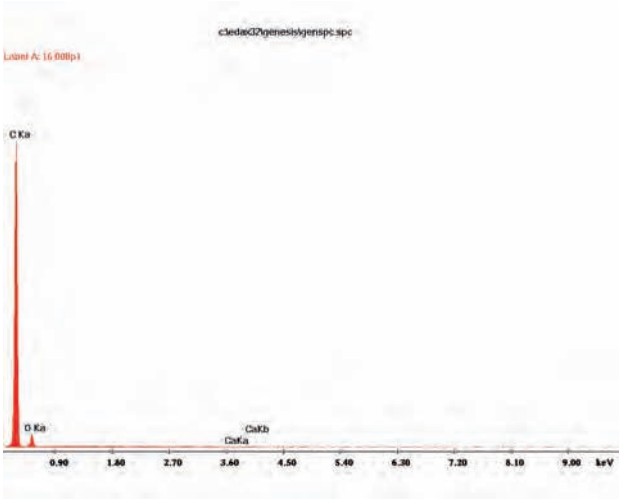


**Fig. 47.** Rusinowo. EDS spectrum obtained for point 1 (Fig. 45)

## Discussion

### Bioapatite and other phosphate phases

*A characteristic of bioapatite*

Bone and antler are built by inorganic and organic substances; the former include bioapatite: carbonated hydroxyapatite, characterized by a very low crystallinity (ie, crystals of a very small size and a defective structure); organic substances include collagen, fats, etc. (Rogóż *et al.* 2009). Some researchers (Pasteris *et al.* 2001) have claimed that bioapatite (studied in mice bone) is almost invariably carbonated apatite. However, this does not apply to all bioapatites: the same researchers have detected a marked concentration of OH groups in the tooth enamel. For bioapatites analysed using the method of Raman spectroscopy, two types of carbonated apatite have been identified, type A and type B, depending on the position of carbonate substitutions and as such, the presence of specific vibrational bands corresponding to the $CO_3$ group (Li, Pasteris 2014, with a list of literature). Bioapatites predominantly represent type B, where the carbonate group replaces the phosphate tetrahedron. In the Raman spectrum, this is manifested by the presence of a band at 1073 $cm^{-1}$.

The chemical composition of a bone, antler and elephant ivory is not essentially different in the type and the number of the main chemical elements (except for dentin, containing a greater concentration of magnesium). Some differences are observed in the microstructure. Apatite in modern antler of reindeer (data on the microstructure of elk antler in given this

study) is better crystallized (has a higher crystallinity index) than in modern bone (Chadefaux *et al.* 2008). The shape of the apatite crystallites is dissimilar: in antler it is needle-like, in ivory and ordinary bone it forms amorphous clusters, all of the above remarks refer to modern, unmodified materials.

*A characteristic of the effects of diagenesis of antler and bone*

The two main components of bone and antler: bioapatite and collagen, may be altered by factors associated with diagenesis (pH, temperature, moisture, microbiological processes, fluctuation of these factors), intentional action (exposure to high heat, chemical processes, eg, softening with organic acids), the age and condition of the animal (Li *et al.* 2015). Studied for a long time and documented in the subject literature these alterations are largely understood at present to be quite complex (Lee-Thorp 2008). Diagenetic processes are thought to contribute to an increase in the crystallinity of bioapatite, its recrystallization and introduction of other ions into the structure of the bone apatite. However, this is not always the rule. The crystallinity index of bioapatite has come to be regarded as a poor indicator of the diagenetic processes, as suggested by a study of apatites in organisms from different geological epochs (Pucéat *et al.* 2004). Biogenic apatite is very finely crystalline and may recrystallize to larger crystals, especially when collagen and other organic components have been forced out (eg, Nudelman *et al.* 2010), eg, by high temperatures. This finds reflection in the shape of infrared spectra and diffraction peaks, and also in features of micromorphology observed under the scanning microscope. In the presence of collagen, the process of recrystallization may be inhibited.

Another method of identification of the diagenetic processes and analysis of their intensity is to study the phase composition of the artefact. Out of all the apatites, biological apatite has the highest content of $CO_3$ groups and the lowest of fluoride. In fossil and magmatic apatites these proportions are reversed (Thompson *et al.* 2011). Among minerals of diagenetic origin the most frequently occurring are calcite, minerals of SiO2 group, pyrite, oxides of iron and manganese, various phosphate minerals. Organic compounds may also occur. These are present on the surface of a bone, filling also the voids (Rogóż *et al.* 2009, 80). Sometimes they are hard to tell apart from intentionally applied layers or fillings. Natural encrustations and fillings built by iron compounds may take form as a result of the degradation of the organic substance surrounding the bone or the object, taking place under conditions of low and moderate oxygen access. The minerals formed in this process include dark grey and black pyrite, amorphous or framboidal (Sawłowicz 2000). Another source of iron may be erythrocyte decay (Rogóż *et al.* 2009, 80). Iron may circulate within the matrix around the bone or an artefact and precipitate on their surface as an effect of changes in pH within an extremely fine subsurface layer, deceptively similar to a layer of paint (Trąbska, Trybalska 2014, 248). There is some contribution to the formation of these mixed, cryptocrystalline phases from microorganisms: one analogue would be the formation of moon milk on cave walls (Gradziński *et al.* 1997). Microorganisms may leave traces of their presence in the form of carboxylic acids or other organic compounds, identifiable via the Raman spectroscopy. In the presence of various cations and anions ($Ca^{2+}$, $Mg^{2+}$, $Na^{+}$, $NH_3^{+}$, $H^{+}$, $PO_4^{3-}$, $CO_3^{2-}$, $SO_4^{2-}$) complex phases may form, known from cave sediments (eg, monetite, ardealite, struvite, stercorite and many other). A phase which is often seen in this environment is brushite ($CaHPO_4 \cdot 2H_2O$).

Analysis of the Ca/P atomic ratio can also bring in information about diagenesis. In antler of modern elk and in modern human bone this ratio is 1.65. A higher value is regarded as the result of the diagenetic substitution of phosphate minerals with calcium, or the effect of the ageing of bone (Li, Pasteris 2014, with a list of literature).

When heated to temperatures of around 100°C in an oxidising atmosphere, apatite loses the carbonate component, this is visible in spectra recorded using the method of infrared spectroscopy (eg, Sukhodub *et al.* 2003)[1]. Low temperature, around 80°C, and an oxidising atmosphere do not alter the shape of the Raman spectrum – the crystallinity of apatite does not change. There is only a decrease in the intensity of some bands from collagen (amide I, amide III, $CH_2$). Furthermore, there is a decrease in the intensity ratio of vibrations v1PO4/CO3 (increase in the carbonate component) (Yamamoto *et al.* 2012). Thus, under conditions of low temperature, thermal alteration of bioapatite may remain undetected. Studies of thermal alterations of bioapatite, derived at temperatures of 100–900°C from a highly mineralized dolphin ear bone, have shown that up to the temperature of 200°C the mineral crystals are preserved. At temperatures 300–600°C their steady (non-stop) disorganization takes place, at 700°C a new phase

[1] As a component of living organisms the carbonate component plays an essential role, influencing certain biological processes (Sukhodub *et al.* 2003, 55).

**Table 6.** Rusinowo. Bands obtained for bioapatites (HA), synthetic hydroxyapatites (HA), fluoroapatite and carbonated apatites type A (ACarbAp) and type B (BCarbAp), and other phosphate: monetite, brushite and phase β-TCP in $cm^{-1}$. Symbols "s", "sh", "m", "w" correspond, respectively to: "strong", "shoulder", „medium" and „weak" (where this data was available in the cited source)

| HA from rabbit bone (Penel *et al.* 2003 | HA laboratory synthesized (Cheng *et al.* 2005) | HA laboratory synthesized (Grossin *et al.* 2010) | HA laboratory synthesized (Penel *et al.* 2003) | HA 1000°C (Sukhodub *et al.* 2004) | F–apatite laboratory synthesized (Comodi *et al.* 2001) | ACarbAp2 laboratory synthesized (Penel *et al.* 2003) | BcarbAp laboratory synthesized (Penel *et al.* 2003) | Antler of modern elk (Li *et al.* 2013) | Assignement of vibrations from (Comodi *et al.* 2001), Penel *et al.* 2003) | Monetite laboratory synthesized (Frost *et al.* 2013) | Natural monetite (Frost *et al.* 2013) | Bone brushite (Penel *et al.* 2003) | β–TCP laboratory synthesized (Penel *et al.* 2003) |
|---|---|---|---|---|---|---|---|---|---|---|---|---|---|
| – | – | 3570 | 3573 | – | – | – | – | – | ν OH– | – | – | – | – |
| – | – | – | – | – | – | – | – | – | – | – | 1171 w | – | – |
| – | – | – | – | – | – | – | – | – | – | 1137 w | 1155 m | – | – |
| – | – | – | – | – | – | – | – | – | – | 1130 w | – | – | – |
| 1103 w | | – | – | – | – | 1106 | – | – | $\nu_1CO_3$ | – | – | – | – |
| – | 1076 sh | 1081 | 1077 | – | 1082 w | – | – | – | $\nu_3PO_4^{3-}$ | 1093 w | 1055 w | 1079 w | 1090 w |
| 1071 w $\nu_1CO_3$ | – | – | 1064 | – | 1066 w | – | 1070 $\nu_1CO_3$ | 1073 | – | 1069 w | – | 1061 w | – |
| – | – | – | 1057 | – | 1054 w | – | – | – | – | – | – | – | – |
| 1044 m | 1044 vw | – | 1048 | 1048 | 1042 m | – | 1045 | – | – | – | – | – | – |
| – | – | – | 1041 | – | – | – | – | – | – | – | – | – | – |
| – | – | – | 1036 | – | 1035 m | – | – | – | – | – | – | – | – |
| 1032 m | – | 1030 | 1029 | – | – | 1031 | 1026 | – | – | – | – | – | – |
| | – | – | – | – | – | 1018 | | – | – | – | – | – | 1016 w |
| 1005 w | – | 1005 | – | – | – | – | 1006 $\nu_3HPO_4$ | – | – | – | – | – | – |
| – | – | – | – | – | – | – | – | – | – | 987 s | 984 s | 988 s | – |
| 961 s | 960 s | 961 | 964 | 961 | 965 s | 957 | 959 | 962 | $\nu_3PO_4^{3-}$ | 953 sh | 965 sh | 970 sh | 971 s |
| – | – | – | – | – | – | 947 | – | – | – | – | – | 948 w | 949 s |

| | | | | | | | | | | | | | |
|---|---|---|---|---|---|---|---|---|---|---|---|---|---|
| – | – | – | – | – | – | – | – | – | – | 898 m | 894 m | – | – |
| – | – | – | – | – | – | – | – | – | – | – | – | 878 m | – |
| – | – | – | – | – | – | – | – | – | – | – | – | – | – |
| – | – | – | – | – | – | – | – | – | – | – | 782 w | – | – |
| 758 v.w. | – | – | – | – | – | 765 | – | – | $\nu_4CO_3$ | – | – | – | – |
| – | – | – | – | – | – | – | – | – | – | – | 703 w | – | – |
| – | – | – | – | – | – | 675 | – | – | $\nu_4CO_3$ | – | – | – | – |
| – | – | – | – | – | – | 630 | – | – | –– | – | 637 w | – | 628 w |
| 611 w | – | 611 | 614 | – | 616 w | – | – | – | $\nu_4PO_4^{3-}$ | 614 w | – | – | – |
| – | – | – | 607 | 607 | 606 w | 608 | 609 | – | – | 606 w | – | – | 609 w |
| 590 w | 589 w | 590 | 591 | – | 591 m | 589 | 590 | – | – | – | – | – | 598 w |
| 584 m | – | 584 | 580 | 584 | 581 w | 579 | 579 | – | – | 588 s | – | – | – |
| – | – | – | – | – | – | – | – | – | – | 573 w | – | – | – |
| – | – | – | – | – | – | – | – | – | – | 560 w | – | – | – |
| – | – | – | – | – | – | – | – | – | – | 549 m | 535 m | – | 546 w |
| – | – | – | – | – | – | – | – | – | – | – | 521 m | – | – |
| – | – | – | – | – | – | – | – | – | – | – | 499 m | – | – |
| – | – | – | – | – | – | – | – | – | – | 470 w | – | – | 473 w |
| 452 | – | 452 | 448 | – | 445 m | 444 | 445 | – | ν2PO43– | – | – | – | – |
| 432 | 428 w | 432 | 433 | – | 430 w | 432 | 432 | – | | 429 w | – | | 437 w |
| – | – | – | – | – | – | – | – | – | – | 416 s | 413 w | – | 405 w |
| – | – | – | – | – | – | – | – | – | – | 391 m | 398 s | – | – |
| – | – | – | – | – | – | – | – | – | – | 374 w | 374 w | – | – |
| – | – | – | – | – | – | – | – | – | – | 327 w | 327 w | – | – |

appears: pure hydroxyapatite. Its crystallinity increases with temperature. At 500°C, the carbonate component is seen no longer (Li *et al.* 2015). In bioapatite from mice bone heated for two hours up to 800–1000°C a very high concentration of OH groups was detected, much higher than in raw bone (Pasteris *et al.* 2001).

A parameter frequently analysed in apatite is its level of crystallinity. This may be estimated by examining bands detected through spectroscopic studies and reflexes obtained from XRD studies (eg, Shift *et al.* 2005). However, their shape does not depend solely on the height of the temperature applied, but also on the duration of this process. The latter factor is practically unidentifiable in the archaeological material. Furthermore, an obvious "sharpening" of bands of XRD reflexes is seen only at around 500°C (for a process lasting 1 hour, Shi *et al.* 2005).

The heating of bone apatite, with an ongoing recording of temperature ranges in which this process could have taken place, can be documented also through analysis of the phase composition of burnt bone or antler (the presence of calcium pyrophosphate, beta and alpha calcium phosphate, Gibson *et al.* 2000).

*Characteristic of studied samples*

Diffractograms (Figs. 1–6, Table 3) reveal in the phase composition of samples from the archaeological object the presence of poorly crystalline hydroxyapatite and chloro-fluoroapatite. In one case (in the white part) calcite was present as well. Other than this, there were no differences between the white and the black (dark grey) parts of the artefact. In the modern antler, we recorded the presence of low-crystalline hydroxyapatite and of a minor amount of quartz (Fig. 1, Table 3). The latter, responsible for providing the antler with strength and rigidity, is visible also on SEM micrographs and in EDS spectra (Figs. 22–27). Clusters of silica and finely crystalline quartz, as well as clusters of hydroxyapatite, are arranged in an alternating pattern (Figs. 24–27). $SiO_2$ was not detected in the ancient artefact because the study was limited to its surface, and sections were not examined. Low-crystalline chloro-fluoroapatite, present in the artefact is diagenetic in origin.

The crystallinity estimated in the hydroxyapatite from the archaeological object as the width of the maxima is slightly lower (broader FWHM of the reflex) than in the antler of modern Eurasian elk (Fig. 48). There may be several reasons for this situation, starting with natural differences between modern and Late Palaeolithic elk. As to whether this difference is statistically significant – this question may be answered only with comparative data for a larger number individuals representing each group. We have no similar data at our disposal. Even if there had been a recrystallization, and formation of secondary apatite, it still continues to be a mineral with fine crystallites and a disorganized structure. The most likely reason for the situation observed here, namely the presence of cryptocrystalline apatite, is survival of collagen in a good condition, something that is visible also in the SEM image (Table 4, Figs. 23, 31, 32).

Also in the SEM image, the bioapatite reveals its cryptocrystalline, homogenous form (Figs. 22–45). The Ca/P ratio is variable, ranging between 1.4 and 7, even within a single sample (PP4). In the modern antler it equals 1 (Figs. 25–27). The variation of this parameter in the apatite sampled from the archaeological object is presumably the effect of the presence of other cryptocrystalline phases: phosphate, carbonate and sulphate phases (cf. below).

On the Raman spectra (Tables 4 and 6, Figs. 7–20, except Fig. 13) was identified moreover the presence of hydroxyapatite, both in the measurement points on the surface of the artefact and in the modern elk antler. The band indicating the presence of carbonate substitutions occurred only at 1070 $cm^{-1}$ which suggests the presence of carbonated hydroxyapatite, type B (samples 2, 2a, 5 and 12), characteristic for bioapatites (cf. above). This band was detected only within the black and dark grey areas, suggesting its association with an organic substance co-occurring with pyrite (see discussion below). The nature of this compound is difficult to explain. Possibly, the substitutions of the carbonate group are secondary, resulting from the proximity of an organic substance. The shape of Raman spectra

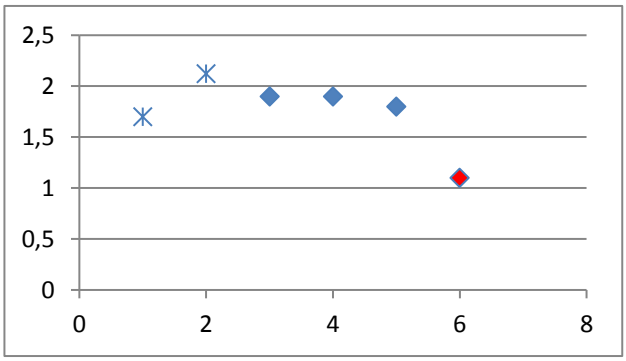


**Fig. 48.** Rusinowo. The degree of crystallinity of hydroxyapatite is based on FWHM measured for 2.8Å reflex (vertical axis, unit 2θ /degree/). Red dot – modern elk antler; asterisks – white fragments of the artefact. other symbols – black surfaces of the prehistoric artefact

does not give a conclusive answer as to whether the bioapatite had been exposed to higher temperatures (eg, around 100°C). Perhaps, this question could be answered through experimental studies.

On the Raman spectrum, the most intensive band for hydroxyapatite occurs around 965 $cm^{-1}$ (vibrations $\nu1PO_4^{3-}$ $cm^{-1}$). Observations of its exact location and width offer insight into the structure of the hydroxyapatite, and thereby, into its alteration induced by diagenetic processes (Thompson *et al.* 2011), and into possible processes of thermal treatment (Sukhodub *et al.* 2003). In the investigated samples, including the modern elk antler, most values of the position of bands from vibrations $\nu1PO_4^{3-}$ $cm^{-1}$ in the tested samples correspond to the values recorded for modern organisms (Thomas *et al.* 2011). Slightly lower values were observed for samples 1 and 6b, with a slightly raised value in sample 9 (Fig. 49). On the other hand, in samples 8 and 10 these values are decidedly higher (Figs. 14, 16, Table 4). The presence of fluoroapatite is not responsible for this increment (Table 6). What is more likely is the presence of secondary phosphate minerals other than hydroxyapatite. They could include monetite ($CaHPO_4$, Frost *et al.* 2013) and/or brushite ($CaHPO_4 \cdot 2H_2O$, Grossin *et al.* 2009) (cf. Table 6). We must be aware that under conditions of low pH many other secondary phosphate phases may take form, but these cannot be identified conclusively in the recorded spectra. Alternately, the high values of the vibrations could result from the presence of vibrations $\nu1SO_4^{2-}$ (983 $cm^{-1}$) (Borzęcka-Prokop *et al.* 2007) which are possible given the presence of pyrite (cf. below). There is no recognizable relationship between the colour of the archaeological object and the position of the vibrational band $\nu1PO_4^{3-}$ $cm^{-1}$.

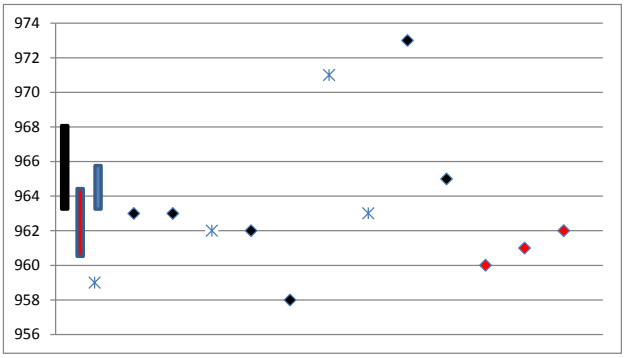


**Fig. 49.** Position of vibrations $\nu1PO_4^{3-}$ $cm^{-1}$ in the analysed samples. Red dots – bioapatite in modern elk antler. Vibrations $\nu1PO_4^{3-}$ $cm^{-1}$ values are marked on the vertical axis. Asterisks indicate samples which represent white areas on the artefact; dark dots – black and blackish-grey areas. The black line at bottom left of the graph represents the position of vibrations $\nu1PO_4^{3-}$ $cm^{-1}$ from geologic apatites obtained from magmatite and fossils (Cretaceous – Oligocene), red line – the position of these vibrations for modern bioapatites from different organisms, blue – the position of analysed bands in fluoride-rich apatites (acc. to Thomas *et al.* 2011)

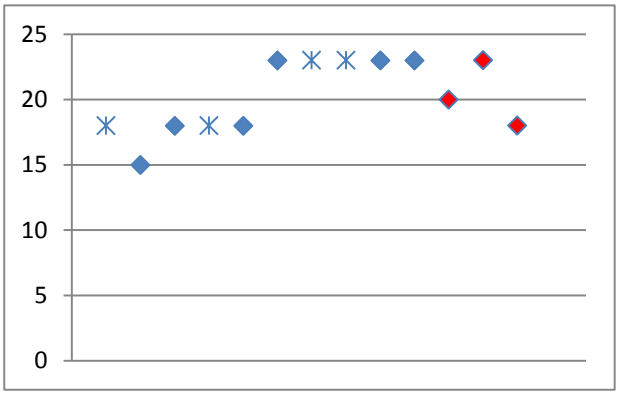


**Fig. 50.** FWHM of band $\nu1PO_4^{3-}cm^{-1}$ (vertical axis). Red dots – hydroxyapatite from modern elk antler; asterisks – samples corresponding to white areas on the artefact; dark dots – dark grey and black areas

In conclusion, the antler may be said to display some minor diagenetic alteration, as suggested by the presence of secondary phosphate minerals, and even more so, by the transformed structure of the bioapatite.

The full width at half maximum parameter from vibrational bands $\nu1PO_4^{3-}$ $cm^{-1}$ corresponds to the values measured in the modern antler. The lower the FWHM value, the larger the crystallites of the mineral (the "sharper" the band). The only divergent sample is no. 2, where the bioapatite has a lower FWHM of the band (Fig. 50), consequently, a slightly more ordered structure. But, this is only a minor divergence, one that does not permit any more far-reaching conclusions. There is no apparent

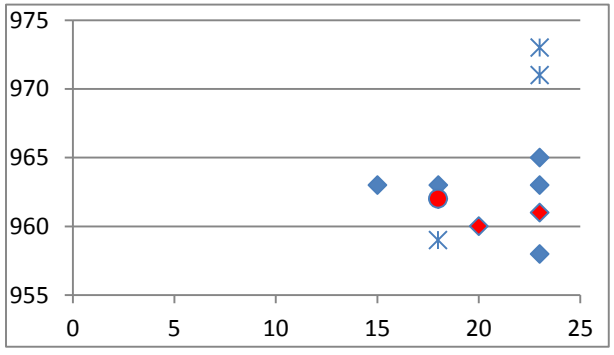


**Fig. 51.** Position of band $\nu1PO_4^{3-}cm^{-1}$ (vertical axis) relative to the FWHM value of this band (horizontal axis). Red dots – bioapatite from modern antler elk; asterisks – samples corresponding to white areas on the artefact; dark dots – dark grey and black areas; red circle – identical result obtained for hydroxyapatite from the artefact and modern elk antler

correlation between the FWHM values and the colour of the surface of the artefact. All of the observed hydroxyapatites are cryptocrystalline, both those from the interior of the antler (as indicated by SEM and XRD studies) and from its surface (Raman studies). The surface of antler had not been exposed to any factors which could have significantly increased or decreased the crystallinity of the hydroxyapatite.

No relationship has been observed between the value of the vibrational bands $\nu_1 PO_4^{3-} cm^{-1}$ and the FWHM parameter (Fig. 51). High values of the vibrations with an attendant low ordering of the hydroxyapatite in samples 8 and 9 suggest coincidence of bands from other phosphate minerals.

The measurements of crystallinity of the hydroxyapatite in XRD analysis and in Raman spectroscopy produced slightly different results (Fig. 48 vs. 50). In the first case greater divergence was observed in the difference in crystallinity of this mineral in the artefact and in modern antler. This is caused by the difference in the size of the area studied via these two methods, and different elements in the structure of this mineral, possibly also by the presence of secondary apatite. In the case of XRD, the analysed area ranges in size between several to a few thousand ångströms of recurring (parallel) elements of the crystalline lattice. In the Raman spectroscopy, the analysed area is in the order of micrometres, and the Raman signal comes from vibrations generated by particular molecules building the structure (Bolewski, Żabiński 1988), (for example, the P-O complex, vibrating differently depending on the energy of its neighbours). In a "local-range" arrangement structure the hydroxyapatite in the artefact and in the modern antler are similar, in the "long range" ordering there are marked differences. Presumably, this is due to the presence of secondary fluoro-chloroapatites. Nevertheless, it is important to note that these differences are minor and may be within the range of error (this is something that might be explained by testing a larger number of samples).

None of the research methods used revealed the presence of phases which appear at a temperature of around 100°C (eg, calcium pyrophosphate $Ca_2P_2O_7$), and in particular, phases β-TCP[2] (700–800°C) and α-TCP (1200°C) (Gibson *et al.* 2000), or structural changes suggesting such an episode.

Within the range, ν4 of 580–620 $cm^{-1}$ were detected distinct bands from the so-called non-apatite groups $PO_4^{3-}$, very poorly crystallized nonstoichiometric apatites which on their surface adsorb water, which element plays an important biological role in bioapatites. The presence of this form of apatite is indicated also by the shoulder of the band at 960 extending towards 950 $cm^{-1}$ (Grossin *et al.* 2009).

[2] Tricalcium phosphate, $Ca_3(PO_4)_2$ (calcium phosphate).

**Collagen and other organic substances**

Collagen (or, more precisely, its different types) is a group of the most widespread mammalian proteins. It is the main component of connective tissue (Hames, Hooper 2009, 52–58), and occurs in abundance in the skin, bones, tendons, and cartilage as well as in antler (Buckley *et al.* 2012). The basic structural units of collagen are three polypeptide strands twisted into a helix stabilized by hydrogen bonds. The polypeptides are composed mainly of glycine, proline, hydroxyproline and hydroxylysine (Hames, Hooper 2009, 54). Many types of collagen exist, at least five have been distinguished (Hames, Hooper 2009, 53), depending on where they form and their role within the organism. The most common, type I, occurs in the connective tissue of bone, skin and tendons (Hames, Hooper 2009, 53). Collagen is subject to denaturation by heating, at temperatures of 40 and 85–95°C (Dong *et al.* 2004, with a list of literature). The protein also becomes degraded by moisture and changes in pH. Some impact on the crystallization of collagen comes from water molecules (Sukhodub *et al.* 2004). In the antler of reindeer the amount of collagen is greater than in bone (ca. 35% vs. 20–30%) (Chadefaux *et al.* 2008).

As a result of diagenetic processes, collagen may, or may not survive (it was not present in samples of microfragments of Palaeolithic antler from the paintings at Lascaux, (Chadefaux *et al.* 2008) and in the bone of Palaeocene bear from Cave Biśnik (Rogóż *et al.* 2009). Its survival is more likely in environments with a moderate and low oxygen access, first of all, at low temperatures (eg, Holmes *et al.* 2005). Under favourable conditions, collagen may survive for even 100 000 years (Lee-Thorp 2008).

Archaeological objects containing collagen can be studied using the method of Raman spectroscopy, and also, mass spectrometry (MS), and in a complementary manner, with other methods as well (eg, SEM/EDS). MS studies proved useful both for identifying and distinguishing between the skin of cattle, sheep and goat found in Danish bog finds of different date (Brandt *et al.* 2014).

The position, intensity and shape of Raman bands from collagen of different animals differ slightly, depending on: i./ the type of animal, and therefore, the composition and the concentration of various amino- and imino acids (Ikoma *et al.* 2003);

ii./ type of collagen in the anatomically and functionally different parts of the animal's body (Buckley *et al.* 2003); iii./ pathological change (Cheng *et al.* 2005); iv./ postdepositional change, such as the presence of molecular water within the collagen (Sukhodub *et al.* 2004); v./ temperature (minor, hard to observe changes were recorded in the collagen of cattle, between -100 and +100°C (Dong *et al.* 2004); vi./ beam laser orientation in relation to the collagen fibrils (Bonifacio *et al.* 2010). Currently, there is no data enabling us to trace the earlier named alterations in the collagen from antler of modern and Late Palaeolithic elk.

The archaeological material and the modern antler subjected to analysis were both found to contain collagen. It is visible in the Raman spectra and in SEM images, in the latter case, as fine fibrils (Figs. 24, 32, 33). Table 4 presents a list and interpretation of vibrations from collagen; Table 7 gives values of Raman vibrations from different kinds of collagen.

In the investigated samples collagen was detected only on the Raman spectra from the antler of modern elk, and in samples 2, 2a and 5. Its presence in sample 9 is not certain. The spectra from modern collagen and from the object from Rusinowo are similar. As was mentioned earlier, the fluctuation of the position of bands from collagen may be due to various reasons. Without reference spectra from elk antler of different ages and condition, and from archaeological antler, it is not possible to conclude as to the causes of this variation in the bands from collagen. It is hard to say if it is due to measurement uncertainty or to some statistically significant cause.

In sample 6b (a dark grey fragment on the surface of the antler) next to gypsum (cf. below) we obtained a very indistinct band at 1329 $cm^{-1}$. Unfortunately, no other bands are visible in the spectrum that could be tied in with this band and in this way to identify the substance which generated the band. It cannot be attributed to silicone (Fig. 21). A substance that may be taken into account would be a simple organic compound, aliphatic in character, or soot (Sadezky *et al.* 2005), or one of the acetates (Ito, Bernstein 1956). This could be a bacterial product (metabolite and/or natural pigment, cf. Jorge-Villar *et al.* 2011). Sample 10 yielded a band which may be ascribed to acetate compounds (919 $cm^{-1}$). It is tempting to look for evidence confirming the presence of an organic sheath inside which the object would have been kept, or of an organic substance used to preserve (decorate) the object. Unfortunately, with the very modest data at hand, we cannot hope to draw any definitive conclusions.

The SEM images also document the presence of clusters of organic compounds, together with iron sulphides. They are characterized either by an irregular, amorphous morphology or take the form of ellipsoidal clusters (Figs. 46, 47). Their nature is unknown.

**Iron sulphides, gypsum, carbonate minerals and manganese compounds**

Inorganic phases, other than the earlier discussed apatite and other phosphate minerals registered in the Raman spectra of the investigated samples from the artefact, include iron sulphides (samples from the Rusinowo artefact, 2, 2a, 3 and 9) and gypsum (sample 6b) (Tables 4 and 8). In the modern antler, these substances were not observed. Clusters of iron sulphides were detected, sometimes jointly with an organic substance, also during the SEM/EDS studies.

Pyrite is the most frequently encountered iron sulphide mineral, eg, in hypergenic conditions. In sedimentary rocks and in the diagenetic zone pyrite forms by way of intermediate, unstable phases: mackinawite (initially, nanocrystalline FeS, and greigite – $Fe_3S_4$). Often, the formation of these phases is stimulated by microorganisms. These phases are regarded as precursors to framboidal pyrite (Sawłowicz 2000). They have been detected on the surface of corroded iron artefacts (Remazeilles *et al.* 2010). Framboidal pyrite, present on the surface of the archaeological object, visible also in SEM images, formed thanks to the presence of iron ions, mobile in a reduced-oxygen or oxygen deficient environment. The source of these ions could have been the natural environment – lacustrine or terrestrial. Concentrations of pyrite presumably appeared thanks to the action of bacteria, something that is possible even in a harsh climate (Wolicka *et al.* 2014).

The tested samples are a mixture of iron sulphides: pyrite, mackinawite with a moderately ordered structure, and iron oxide-hydroxides with mackinawite. Not to be discounted is the presence of greigite. Iron sulphides (chiefly pyrite) occur in the form of framboids (Figs. 28, 29, 33, 34, 36–43). More rarely, they form isolated, scattered crystals (Figs. 44, 45). They are present both in the white and in the black and dark grey areas on the object as streaks and stains, and within the intentionally made grooves (cf. section 3.3.2. in the present subcharter). The framboids of pyrite are accompanied by calcium carbonate (Figs. 36, 37, bands at ca. 1070 $cm^{-1}$ in Raman spectra, Table 4). The agent responsible for the formation of these clusters is anaerobic

**Table 7.** Raman bands [$cm^{-1}$] corresponding to collagen recorded in different organisms. Symbols "s", "sh", "m", "w" correspond, respectively to: "strong", "shoulder", "medium" and "weak" (where this data was available in the cited source)

| Collagen (type I) laboratory synthesized (Cheng *et al.* 2005) | Human collagen (skin) (Cheng *et al.* 2005) | Collagen from rat tendon (Wang *et al.* 2000) | Collagen, 0% RH, rat tendon (Wang *et al.* 2000) | Collagen, 76% RH, rat tail (Wang *et al.* 2000) | Collagen from pig skin (Ikoma *et al.* 2003) | Collagen, from fish scales of *Pagrus major* (Ikoma *et al.* 2003) | Bovine (calf) collagen, (20°C) (Dong *et al.* 2004) | Bovine collagen, (bull tendon) (Bonifacio, Sergo 2010) | Assignement (Cheng *et al.* 2005) | Assignement (Ikoma *et al.* 2003) | Assignement (Dong *et al.* 2004) |
|---|---|---|---|---|---|---|---|---|---|---|---|
| 1664 s | 1665 s | 1684 s | 1663 | 1658 | 1670 s | 1670 s | 1655 | 1665 | Amide I | ν(C=O) amide I | Amide I |
| – | – | – | – | – | 1640 sh | 1642 sh | – | – | – | ν(C=O) amide I | – |
| – | – | – | – | – | 1605 m | 1605 m | – | – | – | Phenylalanine Tyrosine | – |
| – | – | – | 1559 | 1561 | 1586 m | 1585 m | – | – | – | Proline | – |
| 1460 s | 1460 s | 1460 s | 1451 | 1459 | 1451 s | 1450 s | 1443 | 1450 | $CH_2$ $CH_2/CH_3$ | d(CH2) | δ(CH3–CH2) |
| – | – | 1443 sh | – | – | – | – | – | – | – | – | – |
| – | – | 1418 sh | 1408 | 1411 | 1421 sh | 1421 m, sh | – | 10041 | – | νs(COO–) | – |
| – | 1398 sh | 1392 m | – | – | 1387–1393 w | 1387 w | – | – | $CH_2$ | d(CH2) | – |
| – | – | – | – | – | 1340 w, sh | 1340 w, sh | – | – | – | γw(CH2) | – |
| – | – | – | – | – | 1319 m | 1316 m | – | – | – | γt(CH2) | – |
| 1302 s | – | – | – | – | – | – | 1299 | – | $CH_2/CH_3$ | – | δ(CH2) |
| 1266 sh | 1265 sh | 1256 s | – | – | 1269 m | 1268 s | – | 1268 | Amide III | d(NH2) amide III | – |
| 1246 m | 1246 s | – | 1234 | 1243 | 1247 n | 1247 s | – | – | Amide III | d(NH2) amide II | – |
| – | – | – | – | – | 1206 m, sh | 1208 w, sh | – | – | | Tyrosine | – |

| | | | | | | | | | | | |
|---|---|---|---|---|---|---|---|---|---|---|---|
| 1163 sh | 1174 sh | 1166 m | – | – | 1164 w | 1163 w | – | – | Tyrosine | $NH_3^+$ | – |
| 1129 sh | 1126 sh | – | – | – | 1126 w, sh | 1124 w, sh | 1123 | – | ν(C–C) | – | ν(CCC) |
| – | 1099 w | – | – | – | 1093 m | 1097 m | – | – | ν(C–N) | ν(C–N) | – |
| – | – | – | – | – | 1062 m | 1063 m | 1063 | – | – | OH carboxylic group | ν(C–N) |
| 1030 w | 1032 m | – | – | – | 1034 s | 1033 s | – | – | Phenylalanine | Phenylalanine | – |
| 1004 w | 1002 s | – | – | – | 1004 s | 1003 s | 1003 | – | Phenylalanine | Phenylalanine | ν(C–C) Phenylalanine |
| – | – | – | – | – | 972 w, sh | 971 w, sh | – | – | – | – | – |
| – | – | – | – | – | 958 w, sh | 957 w, sh | – | – | – | ν(C–C) | – |
| 937 sh | 937 s | 952 s | – | – | 936 m, sh | 936 m, sh | – | 938 | Proline, Hydroxyproline, ν(C–C) | ν(C–C) | – |
| 918 sh | 918 w | – | – | – | 921 s | 921 s | 917 | 922 | Proline, Hydroxyproline, ν(C–C) | ν(C–C) of hydroxyproline rings | ν(C–N) Proline |
| 873 w | 873 sh | 879 s | – | – | 884 s | 879 m | – | – | Hydroxyproline Tryptophan | ν(C–C) of hydroxyproline rings | – |
| 856 sh | 856 s | – | – | – | 858 s, sh | 855 s | – | – | Proline, Hydroxyproline, Tyrosine | ν(C–C) hydroxyproline rings | – |
| 815 w | 815 m | 822 m | – | – | 816 s | 817 s | 814 | – | Proline, Hydroxyproline, Tyrosine $\nu PO_2^-$ | ν(C–C) | ν(CC) |
| – | 753 w | – | – | – | – | – | – | – | Tryptophan | – | – |
| 667 sh | – | – | – | – | – | – | – | – | Cystine | – | – |
| 646 w | – | – | – | – | – | – | – | – | Tyrosine | – | – |

**Table 8.** Raman vibrations [$cm^{-1}$] corresponding to iron sulphates (pyrite, marcasite, mackinawite and greigite) and gypsum Symbols "s", "sh", "m", "w" correspond, respectively to: "strong", "shoulder", "medium" and "weak" (where this data was available in the cited source).

| Gypsum (Prasad *et al.* 2001) | Gypsum (White 2009) | Assignement (Prasad *et al.* 2001; White 2009) | Pyrite (Kleppe, Jephcoat 2004) | Pyrite (White 2009) | Pyrite – interpretation of vibrations (White 2009) | Marcasite (White 2009) | Greigite (Remazeilles *et al.* 2010) | Greigite (Remazeilles *et al.* 2010) | Nanocrystalline mackinawite (Remazeilles *et al.* 2010) | Crystalline mackinawite (Remazeilles *et al.* 2010) | Fe(III) compounds containing mackinawite (Remazeilles *et al.* 2010) |
|---|---|---|---|---|---|---|---|---|---|---|---|
| 3489 | 3494 w | $\nu_1(H_2O)$ | – | – | – | – | – | – | – | – | – |
| 3401 | 3406 w | $\nu_3(H_2O)$ | – | – | – | – | – | – | – | – | – |
| 1143 | 1136 m | $\nu_3(SO_4)$ | – | – | – | – | – | – | – | – | – |
| 1124 | – | $\nu_3(SO_4)$ | – | – | – | – | – | – | – | – | – |
| 1008 | 1008 s | $\nu_1(SO_4)$ | – | – | – | – | – | – | – | – | – |
| 672 | 671 w | $\nu_4(SO_4)$ | – | – | – | – | – | – | – | – | – |
| 619 | 620 m | $\nu_4(SO_4)$ | – | – | – | – | – | – | – | – | – |
| 495 | 484 m | $\nu_2(SO_4)$ | – | – | – | – | – | – | – | – | – |
| – | – | – | 430 | 430 s | $T_g(3)$ | – | 425 v.w. | – | – | – | – |
| 416 | 415 m | $\nu_2(SO_4)$ | – | – | – | – | – | – | – | – | – |
| – | – | – | – | – | – | 386 s | – | – | – | – | – |
| – | – | – | 379 | 379 s | $A_g$ S–S | – | 376 m | – | – | – | – |
| – | – | – | – | – | – | – | – | 365 s | – | – | – |
| – | – | – | 350 | – | $T_g(1)$ | – | – | 350 s | – | – | 355 m |
| – | – | – | 344 | 343 w | $E_g$, S2 | – | 340 s | – | – | – | – |
| – | – | – | – | – | – | 323 w | – | – | – | – | 322 s |
| – | – | – | – | – | – | – | – | – | – | – | 312 s |
| – | – | – | – | – | – | – | – | – | – | 298 s | – |
| – | – | – | – | – | – | – | – | – | 282 m | – | – |
| – | – | – | – | – | – | – | – | 250 w | – | 260 m | 256 m |
| – | – | – | – | – | – | – | – | – | 208 s | 208 m | – |

[1] Gypsum, pyrite and marcasite from hydrothermal veins and natural methane vents (White 2009).

bacteria which derive energy from the reduction of sulphide minerals, Fe(III) compounds, reduction of organic compounds (presumably supplied by other bacteria, possibly, organic acids, alcohols, acetates, oxalates and others), reduction of nitrates. Products of this activity include carbonate minerals (calcite, aragonite and dolomite), phosphate minerals (apatite) and metal sulphides, sometimes, native sulphur. This bacterial activity has been encountered even in a harsh, Antarctic climate (Wolicka *et al.* 2014).

The joint presence of sulphide phases (pyrite, mackinawite, possibly greigite as well) suggests an almost contemporary formation of framboids responsible for the dark grey hue of the entire object and areas inside the zigzag grooves (cf. section 3.3.2. in the present sub-chapter). The question remains whether the source of the organic substance was natural, or whether it comes from a sheath, or from a staining agent used on the surface of the object. Many organic pigments may survive under waterlogged conditions, and may be present as a result of intentional action or natural processes. The effect of one or the other of these groups (eg, the staining by tannins in the presence of iron) may be undistinguishable, even to sensitive chromatographic methods (Vanden Berghe *et al.* 2009). As noted earlier, the presence of only a single band, at 1329 $cm^{-1}$ (sample 6b) and 919 $cm^{-1}$ (sample 10) is insufficient to draw conclusions about any intentional treatments which could be responsible for the pyrite concentration. The present studies revealed no evidence to postulate the presence of substances of this sort.

Gypsum ($CaSO_4 \cdot 2H_2O$) formed in the process of oxidation of sulphide phases in the presence of calcium ions. This mineral shows no evidence of exposure to high heat, at least not over 90°C. Calcination which could have taken place at lower temperatures is not visible in the Raman spectra (Prasad *et al.* 2001). On the surface of the artefact, gypsum forms irregular white deposits with a yellowish lustre.

It is likely that the vibrational bands approximately at 1070 $cm^{-1}$ mentioned earlier are from calcium carbonate, calcite or aragonite. No other bands from these minerals were observed to assist our diagnosis. It is interesting that these bands were observed only in the black and dark grey areas. Consequently, the presence of these carbonate minerals is related genetically to the presence of pyrite (Wolicka *et al.* 2014). Also present on the surface of the object are encrustations deriving from lake chalk (Płonka *et al.* 2011), but the calcium carbonate recorded by us probably has nothing in common with these formations. Manganese compounds were detected in the SEM image in a small number of cases within the areas of black concentrations. They form irregular, cryptocrystalline clusters (Fig. 46). No iron sulphides, gypsum or manganese compounds were detected in the diffractograms: their concentration was too low.

## Conclusions

Studies of raw antler of modern elk helped identify the microstructure and chemical composition of an unmodified modern raw material and treat it as reference material. Antler is built of bioapatite and collagen. Apatite contains a minor quantity of quartz and iron compounds. Bioapatite is very poorly crystalline. The position of its main Raman band is at 960–962 $cm^{-1}$. Collagen forms fibrils, clearly identifiable in the SEM image. Quartz, perhaps also other forms of $SiO_2$, imparts mechanical strength to the antler. Iron compounds give it a yellowish hue.

Samples extracted from the ancient artefact are characterized by the presence of cryptocrystalline apatite. Its crystallinity is slightly higher than the crystallinity of apatite in modern antler, possibly the result of an error in determination (extremely small sample size!) but also of the level (poor!) of recrystallization of the apatite in the course of the diagenesis. This definitely cannot be the effect of calcination of the artefact – firstly, the disorganization of the apatite is too great, and additionally, the samples were found to contain collagen. The collagen in the modern antler and in the ancient object do not differ.

Samples extracted from the black and dark grey areas on the artefact have very similar characteristics – except for the greater quantity of pyrite in the former; moreover, manganese compounds were detected and lumpy organic compounds (the latter in a small amount), their composition unknown. The pyrite occurred in the form of framboids. Framboids in this part of the object and those observed in the light-coloured part are not the same. Note: when exposed continuously to oxidising conditions the dark areas on the artefact could turn yellow in the presence of oxide-hydroxide compounds of iron. This is something to consider while planning the conditions of a museum display of the object.

Referring to the present studies it cannot be validated that the clusters of framboidal pyrite had formed on the surface of the object due to causes other than natural.

Diagenetic processes affecting the artefact are manifested not only by the presence of framboidal pyrite but also by the occurrence of fluoroapatite, phosphate minerals other than apatite, gypsum and calcite.

No evidence was found of intentional treatment (burning, chemical softening). The same goes for the presence of a sheath made of an organic material.